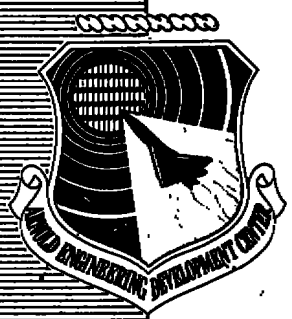

ARTIFICIALLY INDUCED BOUNDARY-LAYER TRANSITION ON BLUNT-SLENDER CONES USING DISTRIBUTED ROUGHNESS AND SPHERICAL-TYPE TRIPPING DEVICES AT HYPERSONIC SPEEDS

A. H. Boudreau
ARO, Inc., a Sverdrup Corporation Company

VON KÁRMÁN GAS DYNAMICS FACILITY
ARNOLD ENGINEERING DEVELOPMENT CENTER
AIR FORCE SYSTEMS COMMAND
ARNOLD AIR FORCE STATION, TENNESSEE 37389

February 1978

Final Report for Period October 30, 1976 – September 30, 1977

Prepared for

ARNOLD ENGINEERING DEVELOPMENT CENTER/DOTR
ARNOLD AIR FORCE STATION, TENNESSEE 37389

NOTICES

When U. S. Government drawings, specifications, or other data are used for any purpose other than a definitely related Government procurement operation, the Government thereby incurs no responsibility nor any obligation whatsoever, and the fact that the Government may have formulated, furnished, or in any way supplied the said drawings, specifications, or other data, is not to be regarded by implication or otherwise, or in any manner licensing the holder or any other person or corporation, or conveying any rights or permission to manufacture, use, or sell any patented invention that may in any way be related thereto.

Qualified users may obtain copies of this report from the Defense Documentation Center.

References to named commerical products in this report are not to be considered in any sense as an indorsement of the product by the United States Air Force or the Government.

This report has been reviewed by the Information Office (OI) and is releasable to the National Technical Information Service (NTIS). At NTIS, it will be available to the general public, including foreign nations.

APPROVAL STATEMENT

This report has been reviewed and approved.

Elton R. Thompson

ELTON R. THOMPSON
Project Manager, Research Division
Directorate of Test Engineering

Approved for publication:

FOR THE COMMANDER

Marion L. Laster

MARION L. LASTER
Director of Test Engineering
Deputy for Operations

REPORT DOCUMENTATION PAGE		READ INSTRUCTIONS BEFORE COMPLETING FORM
1 REPORT NUMBER AEDC-TR-77-120	2 GOVT ACCESSION NO.	3 RECIPIENT'S CATALOG NUMBER
4 TITLE (and Subtitle) ARTIFICIALLY INDUCED BOUNDARY-LAYER TRANSITION ON BLUNT-SLENDER CONES USING DISTRIBUTED ROUGHNESS AND SPHERICAL-TYPE TRIPPING DEVICES AT HYPERSONIC SPEEDS		5 TYPE OF REPORT & PERIOD COVERED Final Report-October 30, 1976 - September 30, 1977 6 PERFORMING ORG. REPORT NUMBER
7 AUTHOR(s) A. H. Boudreau, ARO, Inc.		8 CONTRACT OR GRANT NUMBER(s)
9 PERFORMING ORGANIZATION NAME AND ADDRESS Arnold Engineering Development Center/DOTR Air Force Systems Command Arnold Air Force Station, Tennessee 37389		10 PROGRAM ELEMENT, PROJECT, TASK AREA & WORK UNIT NUMBERS Program Element 65807F
11 CONTROLLING OFFICE NAME AND ADDRESS Arnold Engineering Development Center/DOS, Arnold Air Force Station, Tennessee 37389		12. REPORT DATE February 1978 13 NUMBER OF PAGES 48
14 MONITORING AGENCY NAME & ADDRESS(if different from Controlling Office)		15. SECURITY CLASS. (of this report) UNCLASSIFIED 15a DECLASSIFICATION/DOWNGRADING SCHEDULE N/A

16 DISTRIBUTION STATEMENT (of this Report)

Approved for public release; distribution unlimited.

17 DISTRIBUTION STATEMENT (of the abstract entered in Block 20, if different from Report)

18 SUPPLEMENTARY NOTES

Available in DDC

19. KEY WORDS (Continue on reverse side if necessary and identify by block number)

boundary layer	roughness (distributed)
transitions	spheres
blunt bodies	hypersonic flow
noses	Mach number

20 ABSTRACT (Continue on reverse side if necessary and identify by block number)

Research directed toward establishing criteria for distributed roughness-type boundary-layer trips on blunt-slender cones has been conducted in the AEDC/VKF at Mach numbers from 8 to 13. Results indicate that distributed roughness trips are superior to spherical-type trips in that equally effective distributed roughness trips are one-fifth as high and produce substantially smaller flow-field disturbances. Criteria are defined for

DD FORM 1 JAN 73 1473 EDITION OF 1 NOV 65 IS OBSOLETE

20. ABSTRACT (Continued)

optimum utilization of distributed roughness trips.

AFSC
Arnold AFS Tenn

PREFACE

The work reported herein was conducted by the Arnold Engineering Development Center (AEDC), Air Force System Command (AFSC), under Program Element 65807F. The Air Force project manager was Elton R. Thompson, AEDC/DOTR. The results of the test were obtained by ARO, Inc., AEDC Division (a Sverdrup Corporation Company), operating contractor for the AEDC, AFSC, Arnold Air Force Station, Tennessee, under ARO Project No. V32A-A0A. The manuscript was submitted for publication on November 16, 1977.

CONTENTS

ILLUSTRATIONS

Figure

1.0 INTRODUCTION

Reynolds number is an essential parameter for scaling of aerodynamic data between wind tunnel and free flight. Supersonic and hypersonic wind tunnels usually cannot duplicate the extremely high Reynolds number environment of flight; therefore Reynolds number scaling is employed. Whitfield and Dougherty (Ref. 1) have pointed out, however, that simple scaling based upon direct ratios of Reynolds number may produce errors in the assumption of similitude. They note that "viscous effects are cumulative in the boundary-layer growth on a body and may contain interactions with shock waves and separation as significant features of certain transonic and supersonic flows encountered in modern-day aerodynamic testing. Also, the location of laminar-to-turbulent transition on the body will have possibly significant influence on all of the latter events in the flow."

Experimentalists resort to transition "fixing" by means of artifical tripping devices in order to match the turbulent boundary layers encountered in flight. Whereas a great many devices have been employed as boundary-layer trips, spheres of various sizes have generally become a standard with experimentalists. Spheres offer advantages such as ease of application, uniformity of size, and accurate definability. However, the size of spherical trips (and other similar trips) required to trip the boundary layer has been known to be a strong function of Mach number, increasing rapidly as Mach number increases. This was pointed out some time ago by Potter and Whitfield (Ref. 2) who noted that the ratio of trip height, k, to boundary-layer thickness, δ_k, (i.e., k/δ_k) "increases approximately as the first power of M_e at hypersonic Mach numbers" when transition is fixed at the tripping element. This means that in hypersonic flow the trip is usually as large as, or larger than, the boundary-layer thickness; therefore, the flow field outside the boundary layer is disturbed as well. Usually, one can observe strong shock waves emanating from boundary-layer trips under hypersonic conditions. While experimentalists justify the use of such large trips by the requirements for turbulent boundary-layer similitude, flow-field analysts question the validity of test results when the flow-field disturbances are present. Sterrett et al., Ref. 3, have presented evidence that flow-field disturbances can be manifested far downstream of the tripping elements despite some indications that the boundary layer is turbulent and free of trip-induced anomalies. Their results are shown in Fig. 1 where the development of a hypersonic boundary layer on a flat plate is illustrated. The tripping elements (spheres, $k/\delta_k = 1.6$) produce noticeable anomalies in the boundary layer for approximately 20 sphere diameters downstream of the trips as shown by the oil flow photograph. Aft of that point (i.e., 20 k downstream of the spheres) an apparently normal turbulent boundary layer is established judging from the oil flow photograph and heat-transfer-rate measurements which indicate a turbulent level. When a compression surface is encountered some 173 k downstream of the trips, disturbances reappear in the boundary layer. This is remarkable considering that a separation region exists just forward of the wedge.

It becomes obvious, therefore, that boundary-layer trips need to be reduced in size while maintaining their effectiveness. One method of achieving this is through the use of "distributed roughness" trips. This class of tripping device consists of tripping elements in close proximity to one another and extending over a relatively large area of the model. Examples of such trips are "grit-blasted surfaces" where the model is roughened by the impact of hardened steel grit air blasted onto the surface, and "distributed grit" where grit particles are bonded to the model with adhesives. Previous tests at the Arnold Engineering Development Center (AEDC) von Kármán Gas Dynamics Facility (VKF) have successfully employed grit-blasted surfaces and distributed grit to achieve turbulent boundary-layer flow on very blunt bodies. Also, unpublished data from VKF Hypervelocity Wind Tunnel (F) (Tunnel F) have demonstrated that a 0.0035-in. peak-to-valley surface roughness could adequately trip the boundary layer on a hemisphere cylinder as shown in Fig. 2. However, very little work has been done with distributed roughness on blunt-slender cones, the configuration of greatest practical interest in hypersonic testing today. The vast majority of tripping experiments have been carried out on flat plates, sharp cones, and hollow cylinders as indicated by Pate, Refs. 4 and 5. Also, no systematic investigation has been conducted to date on distributed roughness as boundary-layer trips for wind tunnel testing.

The VKF Boundary-Layer Trip Study was instituted at the AEDC-VKF to address these needs. The objectives of this research were to:

1. Examine distributed roughness-type trips such as grit-blasted surfaces, distributed grit glued to model surfaces, and machined type roughnesses;

2. Conduct an experimental program where such distributed roughness trips would be compared to the classical spherical trips, and

3. Correlate past and present results.

The experimental program consisted of entries in VKF Hypersonic Tunnel (B) (Tunnel B) in May 1977 where Mach 8 data were obtained and in VKF Tunnel F in April 1977 where Mach 13 data were obtained. This report covers results from these test.

Future work in this research effort will include detailed examination of flow-field disturbances caused by distributed roughness and spherical-type trips, examination of flow fields and tripping requirements for more complex shapes, and refinement of correlation techniques.

2.0 EXPERIMENTAL APPARATUS

2.1 VKF TUNNEL B

Tunnel B (Fig. 3) is a closed circuit hypersonic wind tunnel with a 50-in.-diam test section. Two axisymmetric contoured nozzles are available to provide Mach numbers of 6 and 8; and the tunnel may be operated continuously over a range of pressure levels from 20 to 300 psia at $M_\infty = 6$ and 50 to 900 psia at $M_\infty = 8$, with air supplied by the VKF main compressor plant. Stagnation temperatures sufficient to avoid air liquefaction in the test section (up to 1,250°R) are obtained through the use of a natural-gas-fired combustion heater. The entire tunnel (throat, nozzle, test section, and diffuser) is cooled by integral, external water jackets. The tunnel is equipped with a model injection system which allows removal of the model from the test section while the tunnel remains in operation. A description of the tunnel may be found in the Test Facilities Handbook (Ref. 6).

The Tunnel B entry was conducted at Mach 8 at stagnation pressures from 446 to 860 psia which produced free-stream unit Reynolds numbers from 2.0×10^6 to 3.7×10^6 per foot.

2.2 VKF TUNNEL F

Tunnel F (Fig. 4) is an arc-driven wind tunnel of the hotshot type (Refs. 6 and 7) and capable of providing Mach numbers from about 7 to 13 over a Reynolds number per ft range from 0.20×10^6 to 50×10^6. Test are conducted in a family of contoured nozzles. The three axisymmetric, contoured nozzles have 25-in., 40-in., and 48-in. exit diameters, which connect to the 54-in.-diam test station and provide a free-jet exhaust. Nitrogen is used for aerodynamic and aerothermodynamic testing, and air is used for combustion testing. The test gas is confined in either a 1.0-cu-ft, 2.5-cu-ft, or a 4.0-cu-ft arc chamber where it is heated and compressed by an electric arc discharge. The increase in pressure results in a diaphragm rupture with the subsequent flow expansion through the nozzle. Test times are typically from 50 to 200 msec. Shadowgraph and schlieren coverage is available at both test sections.

This test was conducted using the 48-in.-exit-diam contoured nozzle in the 54-in.-diam test section to obtain a nominal free-stream Mach number of 12.5. Nitrogen was the test gas. The 4-cu-ft arc chamber was used, and useful test times up to approximately 100 msec were obtained. Because of the relatively short test times, the model wall temperature remained essentially invariant from the initial value of

approximately 540°R, thus $T_w/T_{o_\infty} \cong 0.15$ to 0.25 which approximates the condition of practical interest for reentry vehicles. An installation sketch is provided in Fig. 5.

2.3 MODEL

The test article was a 7-deg half-angle cone with a sharp cone length of 48 in. This model, shown in Fig. 6, features ten interchangeable noses which provide a sharp nose and blunt nose radii, r_n, of 0.295, 0.589, and 2.187 in. plus variations in the type of distributed rougheness trips. The model was instrumented with up to 66 heat-transfer gages for both the Tunnel B and Tunnel F tests. The Tunnel F tests also included pressure measurements on the model. Twenty-three spherical trip rings were available at six model stations, providing several trip heights at each station. The sharp, 0.295-in. and 0.589-in.-radius noses are shown in Fig. 7a. Examples of smooth (nominal 32-μin. finish), applied grit, grit blasted, and numerically controlled machined (NCM) surfaces are shown. A blown-up view of the 25-mil NCM nose is presented in Fig. 7b. Each tripping element is a pyramid with a total height (peak-to-valley) of 25 mils. The base plane of the pyramids is recessed 1/3 k below the original

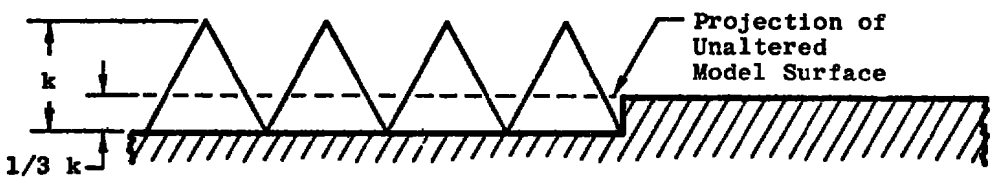

unaltered model surface as shown in the sketch. While these NCM noses are very durable, they are much less cost effective than the applied grit on a smooth nose. Such NCM noses typically required 100 manhours of machine shop work. The NCM noses were constructed of aluminum, whereas the model and the other noses shown in Fig. 7a were constructed from 1300 series stainless steel. The r_n = 2.187-in. nose is shown in Fig. 7c with 25-mil applied grit bonded to the surface. The distribution of grit in this photograph is typical of that used during the tests.

2.4 INSTRUMENTATION

Coaxial surface thermocouple gages were used to measure the surface heating rate distributions. The coaxial gage consists of an electrically insulated Chromel® center conductor enclosed in a cylindrical constantan jacket. After assembly and installation in the model, the gage materials are blended together with a jeweler's file. This results in thermal and electrical contact between the two materials in a thin layer at the surface of

the gage, i.e., a surface thermocouple. A second result of filing the gage surface is the opportunity for "perfect" contouring of the gage to the model surface, a fact that is important for transition studies since no measurable steps or gaps are introduced by the gages.

In practical measurement applications, the surface thermocouple behaves as a homogeneous, one-dimensional, semi-infinite solid. The instrument provides an electromotive force (EMF) directly proportional to surface temperature which may be related by theory to the incident heat flux. All heat-transfer gages were bench calibrated prior to their installation into the model. The precision of these calibrations is estimated to be ±3 percent. The gages were supplied and installed by VKF.

Model pressures for the Tunnel F tests were measured with internally mounted pressure transducers built and installed by VKF. For pressures greater than 1 psid, a wafer-style semiconductor strain-gage transducer with a sealed reference port was used. For pressures less than 1 psid, a similar wafer transducer was used with the reference port at near vacuum pressure. The wafer transducer is nominally 0.56 in. in diameter by 0.35 in. thick. Application of a differential pressure produces a force on the metal diaphragm. The diaphragm is instrumented with two semiconductor strain gages which sense the deflection.

The test section of Tunnel F was instrumented to monitor the tunnel conditions. This instrumentation consisted of two hemisphere cylinder probes instrumented with coaxial heat-transfer gages, two pitot pressures, and four static pressure transducers installed at Sta 372 in the 48-in.-diam nozzle.

The diameter of the hemisphere cylinder heat probes was selected as the maximum size that would still have a laminar boundary layer at the shoulder gage locations. This criterion dictated a 1-in. diameter for the $M_\infty = 12.5$ test conditions. The hemisphere cylinders were instrumented with coaxial surface thermocouples to measure the heat-transfer rate at the stagnation and shoulder location. The pressures were obtained using standard strain-gage transducers developed at VKF. The heat probes and pitot pressure probes were mounted at an appropriate distance from the model to eliminate shock interference.

All instrumentation discussed was developed at AEDC specifically for Tunnel F applications. Further description and discussion can be found in Refs. 7, 8, and 9.

The Tunnel B stilling chamber pressure was measured with a 1,000-psid transducer referenced to a near vacuum. Based on periodic comparisons with secondary standards, the uncertainty (a bandwidth which includes 95 percent of residuals) of the transducers is

estimated to be within ±0.1 percent of reading or ±0.5 psi, whichever is greater for the 1,000-psid range. Stilling chamber temperature measurements were made with Chromel®-Alumel® thermocouples which have an uncertainty of ±1.5°F + 0.375 percent of reading, based on repeat calibrations.

3.0 PROCEDURES

3.1 TEST CONDITIONS

The Tunnel B tests were conducted at a nominal free-stream Mach number of 8 and several (six) different free-stream unit Reynolds numbers. Reservoir pressure, P_o, was varied along with reservoir temperature, T_{o_∞}, in accordance with previous detailed calibrations to yield variations in Reynolds number. Nominal test conditions were:

M_∞	P_o, psia	T_{o_∞}, °R	q_∞, psia	p_∞, psia	T_∞, °R	Re_∞/ft x 10^{-6}
8.0	860	1343	3.94	0.088	97	3.75
	770	1327	3.53	0.079	96	3.42
	670	1323	3.09	0.069	96	3.00
	614	1316	2.84	0.063	96	2.77
	559	1324	2.57	0.058	96	2.49
	446	1323	2.07	0.047	96	2.00

The method of determining the tunnel flow conditions in Tunnel F is briefly summarized as follows: instantaneous values of nozzle static pressure and pitot pressure (P_o') are measured, and an instantaneous value of the stagnation heat-transfer rate ($\dot{q}_o$) is inferred from a direct measurement of shoulder heat rates on the hemisphere cylinder heat probes. Total enthalpy (h_o) is calculated from P_o' and $\dot{q}_o$ and the heat probe radius, using Fay-Riddell theory, Ref. 10. The free-stream static pressure is obtained from the nozzle static pressures in a correlation determined from previous detail tunnel calibrations. The Mach number is calculated from the isentropic relationship using the test section pitot pressure and static pressure.

The centerline pitot pressure on the test model, the Mach number, and h_o are then used to calculate the free-stream conditions from isentropic flow equations and the normal shock relationships. The isentropic reservoir conditions are read from tabulated thermodynamic data for nitrogen (Ref. 11 using h_o and s_∞/R. The equations for this procedure are contained in Refs. 12 and 13.

Test conditions for Tunnel F were:

M_∞	P_o, psia	T_{o_∞}, °R	q_∞, psia	p_∞, psia	T_∞, °R	$Re_\infty/ft \times 10^6$
12.5	6,800 to 15,500	2,100 to 3,500	5.7 to 9.5	0.04 to 0.10	88 to 126	3.0 to 6.0

3.2 TEST PROCEDURES

The primary variables for the experiments in both Tunnels B and F were Reynolds number and trip configuration. Angle of attack was maintained at zero, and model wall temperature ratios (T_w/T_{o_∞}) remained relatively constant at 0.42 for Tunnel B and 0.15 to 0.25 for Tunnel F.

3.3 DATA ACQUISITION AND REDUCTION

The Tunnel F model data (pressure and heat-transfer rate) and the tunnel monitor probe data were recorded on the Tunnel F Transient Data System (TDS). The TDS is capable of scanning the 100 available data channels at preselected rates (normally 100,000 samples/sec). Data for an entire run were stored on the disk unit of a PDP 11/40 Computer which is an integral part of the TDS. The run data plus calibration results and model constants are transmitted to an offline digital computer for final data reduction.

Since Tunnel F operates with a constant volume reservoir with an initial charge density, the reservoir conditions decay with time. As a result, all tunnel conditions and model data results vary with time during the useful data range. Nondimensional values such as M_∞ and model pressure/p_o' are relatively constant with time. Timewise variations in Reynolds number permit acquisition of data at different Reynolds numbers for the same run.

During the Tunnel B tests the outputs of the model coax gages were monitored continuously so that before each test run the model temperatures were less than 80°F, and the uniformity of temperature was less than ±5°F. The model was then injected at the desired test attitude, taking about 2 sec to reach tunnel centerline, and remained on centerline approximately 4 sec before initiation of model retract. The instrumentation output was recorded continuously from liftoff until the model began moving out of the tunnel at retract. After each test run, the model was cooled and prepared for a subsequent injection. The gage outputs were recorded on magnetic tape using a Beckman® 210 analog-to-digital converter. Each gage was recorded approximately 17 times per second. Data reduction was performed by an online digital computer.

4.0 DATA PRECISION

4.1 TEST CONDITIONS UNCERTAINTY

Uncertainties in the basic tunnel parameters for Tunnel B have been estimated from repeat calibrations of P_o and T_{o_∞} instruments and from the repeatability and uniformity of the tunnel flow during calibrations. The parameters P_o, T_{o_∞}, and Mach number, with their uncertainties, were then used to compute the uncertainties in the other parameters dependent on these by means of the Taylor series method of error propagation. These uncertainties are listed below:

	Uncertainty (±), percent				
M_∞	P_o	T_{o_∞}	T_∞	P_∞	Re_∞/ft
0.3	0.1	0.4	0.7	1.6	1.1

For the Tunnel F tests, laboratory calibration using static loads indicates that the pressure transducers are accurate to within ±1 percent. Similarly, the uncertainties in the heat-transfer-rate gages are ±5 percent. The uncertainties in measured data, however, are higher because the dynamics of the measurements and system errors. The uncertainties in the monitor probe measurements (P_o' and $\dot{q}_o$) were estimated considering both the static load calibrations and the repeatability of the test section pitot profiles. The uncertainty in the pressure data (P_o') is estimated to be ±3 percent, based on an average of two measurements. The heat-transfer-rate ($\dot{q}_o$) uncertainty is ±5 percent based on an average of four measurements. The uncertainty in the Mach number determined from monitor measurements during each run is ±3 percent. These values along with the results from the tunnel calibration were used to estimate uncertainties in the tunnel flow parameters. Representative values are given below.

Uncertainty (±), percent			
M_∞	P_∞	T_∞	Re_∞/ft
3	7	8	11

4.2 MODEL DATA UNCERTAINTY

The errors introduced into the heat flux calculations of Tunnel B data from the surface temperature-time histories by assuming the solution for a homogeneous, one-dimensional, semi-infinite solid applies for the coax gage of finite length have been examined by comparing semi-infinite and finite slab solutions for an exposure time

equivalent to the actual test data. These comparisons showed the semi-infinite solution produced results up to three percent too high, and should be interpreted as a bias error. Random error is introduced by the amount of noise on each measurement channel. Although a statistical analysis was not made for each gage, the following tabulation is a good representation of this type error for all gages:

$\dot{q}$ Range, Btu/ft^2-sec	$\dot{q}$ Uncertainty (±), percent
> 5	9
1-5	11
0.5-1.0	25

The uncertainty estimates for the model heat-transfer rate and pressure data in Tunnel F are given below in terms of the absolute level measured. The reference heat-transfer rate, $\dot{q}_o$, uncertainty is ±5 percent and P_o' is ±3 percent. Therefore, the uncertainty of the nondimensional ratio $\dot{q}/\dot{q}_o$ and P/P_o' by the Taylor series method of error propagation yields the following:

$\dot{q}$ Range, Btu/ft^2-sec	Uncertainty (±), percent	
	$\dot{q}$	$\dot{q}/\dot{q}_o$
> 1	9	10
2.0 - 1.0	14	15

p Range, psia	P	P/P_o'
>0.5	5	7
<0.5	10	11

5.0 RESULTS AND DISCUSSION

Van Driest and Blumer, Ref. 14, have presented an example of the effects of boundary-layer trips on the location of transition. Their example, shown in Fig. 8, plots the location of the end of transition (the point where fully turbulent flow exists) versus Reynolds number. Here x_t is the surface distance from a sharp nose to the end of transition and s_t is the blunt nose surface distance to the end of transition. In this example, x_t moves toward the nose of the cone in a continuous manner for the smooth wall case. For the tripped case, however, the forward movement of x_t is markedly

different. Three distinct regions may be defined for the curve which represents the tripped case. In region (1) x_t is moved slightly forward by the trip; however, the transition location is primarily established by local flow conditions and free-stream disturbances. This is esentially an area unaffected by the trips. Region (2) is characterized by a rapid forward movement of x_t for a correspondingly small change in Reynolds number until the point "A" is reached, which van Driest and Blumer have defined as the "effective point." In region (3) the roughness element is predominant in establishing the transition location (see Pate, Ref. 4), and further increases in Reynolds number yield only a gradual movement of transition toward the tripping element. For hypersonic conditions, extremely high Reynolds numbers or extremely large trips may be required to bring x_t to the trip position, or near it (point B on the curve). The shape of the "tripped curve" in Fig. 8 and the location of the "effective point" are functions of the type and location of the tripping device used, as well as the type of body being considered.

The distance x_t or s_t may be determined by many methods. The experiments described herein used heat-transfer-rate measurements along the model surface to determine transition location. Early work in this area by Potter and Whitfield, Ref. 2, has shown that the point at which the surface temperature (or heat-transfer rate) reaches a peak on a flat plate in supersonic flow corresponds to a point near the end of the transition region. More recently, Demetriades (Ref. 15) compared various methods of transition detection on a 5-deg half-angle sharp cone at Mach 8 in VKF Tunnel B. His results would suggest that the peak heat-transfer rate on conical bodies at hypersonic velocities corresponds to the end of the transition zone, i.e., the area where fully turbulent flow is established. With these results in mind, the point at which a fully turbulent boundary layer is established will be defined as that point at which the heat-transfer rate reaches a peak or levels off to agree with turbulent theory after a rise from the laminar level. It is that point that we shall designate as x_t or s_t. This conclusion is well supported by a comprehensive review and correlation of transition location by Pate, Ref. 5. In determining x_t or s_t for the present tests, the experimental heat-transfer rates were compared to rates predicted by VKF laminar and turbulent boundary-layer theory (Ref. 16) as shown in Fig. 9. In this figure the distributed roughness data (open symbols) indicate a fully developed turbulent boundary layer over the entire body, whereas the spherical trips located at $s/r_n = 33$ yield a turbulent level at an s/r_n around 50 which corresponds to $s_t = 30$ in. The distributed roughnesses normally extended to $s/r_n = 5$ ($s = 3$ in. for the $r_n = 0.589$-in. nose); therefore, no valid data were available forward of 3 in.

In order to validate transition results per se, the 7-deg cone was tested both in Tunnel B and in Tunnel F with a sharp nose. The results are compared to prediction obtained using the well-known correlation of Pate (Refs. 5 and 17) in Fig. 10. Good agreement is noted.

Basic results from the r_n = 0.589-in. nose on the 7-deg cone at Mach 8 are presented in Fig. 11. Here s_t (the surface distance to the end of transition) is plotted versus free-stream unit Reynolds number. This figure compares the classical spherical trips with distributed roughness-type trips. Stainback, Ref. 18, concludes that: "The laminar boundary layer can be tripped to produce turbulent flow on a blunt conical model and the values of the ratio of roughness height to boundary-layer displacement thickness k/δ_k^* required to accomplish this effect range from 1.7 to 2.2 when the roughness is located well downstream (s/r_n = 13→20) from the spherical nose." He also noted that when k/δ_k^* = 2.7 to 3.5 "a nonuniform circumferential heat-transfer rate is produced on the model downstream of the roughness element" for more than 20 in. Therefore, in the present tests, single-row spherical trips spaced 4 k apart and having a height 2 δ_k^* were placed at various s/r_n locations to determine what effects axial location might have. The results of Fig. 11 clearly indicate that one should place the trip around s/r_n= 6 for the present case. A 2 δ_k^* trip at s/r_n = 3 did not trip the boundary layer. This point will be discussed in more detail later in this report in relation to both distributed roughness and spheres. A double row of 2 δ_k^* high spheres actually produced a slight rearward movement of s_t, although the difference is within the accuracy of measurement. Stainback, Ref. 18, also found that a double row of spheres was essentially equivalent to a single row. When a triple row of 2 δ_k^* high trips was used, however, a 4-in.-forward movement of s_t was noted which was roughly equivalent to a single row of 4 δ_k^* high trips at s/r_n = 3. The 4 δ_k^* spheres (0.063-in. diameter) and the triple row 2 δ_k^* spheres (0.025, 0.063, and 0.078-in. diameter) are contrasted with the relatively small 14-mil distributed roughness results where s_t is at most 3 in. from the stagnation point at $Re_\infty/ft = 3.7 \times 10^6$. As noted previously, accurate measurements of heat-transfer rate were not obtained in the distributed roughness region, hence s_t = 3 in. is the minimum determinable end of transition location. Note that the 14-mil NCM roughness and the 14-mil applied grit roughness results are essentially identical. Hence one can use either NCM roughness or applied grit as a distributed roughness trip with essentially equivalent results based on these trip configurations. While most of the distributed roughness trips extended to an s/r_n of 5, some data points were obtained with grit extending beyond that point. Note that by extending the grit to s/r_n = 10 a more effective trip is realized. Also shown in Fig. 11 are results from the 25-mil NCM nose which indicate that the 7-deg cone model was tripped to fully turbulent flow (i.e., s_t = 3 in.) at a free-stream unit Reynolds number of only 3.2×10^6 per foot.

The spherical trip results of Fig. 11 are further analyzed in Fig. 12 where the variation of the end of transition, s_t, with the ratio k/δ_k^* is compared to the correlation of Potter and Whitfield (Ref. 19). Coats, Ref. 20, when speaking about the Potter-Whitfield correlation (in regards to Coats' very blunt bodies) stated: "A note of caution must be included regarding the validity of this or any two-dimensional correlation

for bodies less blunt than those of the present investigation. The inviscid entropy layer discussed earlier may be a significant factor in the application of two-dimensional trip sizing techniques to such configurations. The very blunt noses of the present investigation produce thick entropy layers which are not believed to significantly affect either natural or induced boundary-layer transition, aside from the reduction in local Mach and unit Reynolds numbers; thus the two-dimensional techniques would be expected to be applicable. Conversely a slightly blunted body has a thin entropy layer with proportionally larger entropy gradients which must alter the boundary layer. Under these circumstances the two-dimensional techniques may not be applicable since they do not in any way account for the complicated flow resulting from absorption of the entropy layer by the boundary layer." One should note, however, that the Potter-Whitfield method adequately predicts s_t while always yielding a conservative answer. The experimental data of Fig. 12 indicate that a k/δ_k^* of 4 is required to bring s_t up to, or near, the trip. This differs with Stainback's conclusion that $k/\delta_k^* = 2$ is adequate for effective tripping. Evidently the criteria for effective tripping are more complicated than a mere δ_k^* criterion. As will be noted later, the pressure gradient has a significant influence on the trip size required and Stainback's results were for $s_k/r_n = 13$ to 20 where the gradient is relatively small. An important advantage of the Potter-Whitfield method (in comparison to other correlations) is that s_t may be defined as any point between the natural transition location and the trip. If s_t is predefined, a trip size may be determined which is significantly smaller than that required for transition to occur at the trip. For instance, the experimental data indicate that by decreasing the spherical trip size from $k/\delta_k^* = 4$ to 2, the end of transition, s_t, moves back to a point 18 in. aft of the stagnation point. This may be satisfactory in many applications. Note also that the k/δ_k^* ratio for effective distributed roughness trips (when δ_k^* is taken at $s/r_n = 6.5$) is only 0.55 at this location.

Results from the 7-deg cone with nose radii, r_n of 0.295 in. and 2.187 in. are compared to the $r_n = 0.589$-in. results in Fig. 13. Spherical trips placed at $s/r_n = 13$ yield essentially identical results for the $r_n = 0.295$-in. and 0.589-in. noses. The $r_n = 0.295$-in. transition location is 4 in. forward of the $r_n = 0.589$-in. location, but this is to be expected since the 0.063-in. trips used were 2.2 δ_k^* instead of 2.0 δ_k^*. The distributed roughness results, however, indicate that the 0.295-in.-radius nose is much more sensitive to variations in unit Reynolds number. The large nose ($r_n = 2.187$ in.) results are indicated by open symbols and show that the large radius greatly aids the distributed roughness tripping. Grit was gradually removed from the stagnation region of the large nose in three steps in order to determine an optimum starting point for the distributed roughness. Note that the difference in s_t between the 10-deg and 45-deg starting points is only 0.6 in., whereas the difference between 45-deg and 65-deg is more than twice that length. These data and other experience on the $r_n = 0.589$-in. nose tend to point to a

45-deg starting location as being close to optimum. This result seems logical since the 45-deg location also corresponds to the area of maximum local Reynolds number on a hemisphere nose.

Tripping results at Mach 12.7 in VKF Tunnel F are presented in Fig. 14. Although the trends are similar to the Mach 8 results, one notes a shift to higher values of unit Reynolds number in order to achieve effective tripping. While such strong Mach number effects are well known for the case of spherical tripping, these data suggest that the Mach number effects on distributed roughness type trips are equally strong. Note that the double-row 4 δ_k^* high spherical trips (at s/r_n = 3 and 6) give results similar to the 14-mil distributed roughness trips as was the case at Mach 8. The fairings marked "Conical Sec. Only" represent results from noses where grit was applied starting at approximately 75 deg from the stagnation point and extending to s/r_n= 5. The fact that these results agree with the other distributed roughness results (within data repeatability) indicates that the tripping effect of grit on the hemisphere section is much less important when compared to grit on the conical section. A run with applied 14-mil grit only on the hemisphere section of the nose produced results falling along the ineffective tripping line at a Reynolds number of 4.8×10^6 per foot.

Having determined that the conical section of the r_n = 0.589-in. nose was most important for effective distributed roughness tripping, tests were conducted at Mach 8 to determine how far the grit should extend along the conical section. Figure 15 presents results on the r_n = 0.589-in. nose. Here the nondimensional surface distance to the end of transition, s_t/r_n, is plotted against s/r_n to the end of the grit coverage. The results shown are, of course, a strong function of Reynolds number, and by varying Re_∞/ft one could generate a family of such curves. These results, however, do point out that the distributed roughness trip becomes more effective as the grit is extended rearward. Note that the end of transition reaches the end of the grit at approximately s/r_n = 11.5. By examining the pressure distribution along the surface (Fig. 16) one can observe that this roughly corresponds to the bottom of the commonly termed "pressure bucket", i.e., the area of minimum surface pressure.

From the results presented thus far, and by examining Fig. 16, one can gain insight into the behavior of the distributed roughness tripping mechanism. Optimum tripping is evidently obtained when one begins the roughness area at approximately 45 deg (as indicated by Fig. 13) and extends the roughness as far toward the bottom of the pressure bucket as practical (as shown in Fig. 15). Most of the distributed roughness results of the present study used roughness extending to s/r_n = 5, which, according to Fig. 16, has a pressure 40 percent above the bucket value. As noted in Fig. 11, an advantage was seen in extending the grit to s/r_n = 10 which has a pressure within ten percent of the bucket value.

To trip the boundary layer in the nose region of a blunted cone, one must contend with the strong favorable pressure gradient in that area. This pressure gradient tends to maintain the boundary layer in a laminar state and will actually "relaminarize" turbulence generated near the stagnation point. This can happen even when surface roughness is present as shown by the data in Fig. 2 where, at an s/r_n of 1.6 or 1.8, the heat-transfer level drops from a previously turbulent value to a transitional value. The phenomenon has been termed "Laminarization" by Launder and Jones, Ref. 21, and has been observed for many years by experimentalists. Therefore, in order to trip the boundary layer. the trip size must increase relative to the boundary-layer thickness as one progresses towards the stagnation point from the "bucket", i.e., the ratio of k/δ_k^* must increase in order to overcome the expansion aft of the trip location. This conclusion is supported by the data of McCauley, et al. ((Ref. 22), who found that k/δ_k^*'s on the order of 25 were required for spherical trips located 45 deg off the stagnation point and that "k/δ_k^* effective" decreased as the trips were moved aft. As previously noted in Fig. 12, k/δ_k^* need be only 4 or less for effective spherical-type trips located at $s/r_n = 6.5$. Hence one cannot simply speak of trip size in terms of k/δ_k^*, especially when strong favorable pressure gradients are present. As previously mentioned, distributed roughness trips offer an advantage of much smaller sizes than spheres; however, the tripping mechanism must somewhat follow that of the spherical-type trips. The distributed roughness tripping elements in the forward section of the roughness area evidently trip the boundary layer since they have a relatively high ratio of k/δ_k^* at that point. This is caused by the displacement thickness being relatively thin on the nose section and increasing in thickness rapidly as the expansion progresses onto the conical section. After the initial tripping the relatively small roughness apparently "maintains" the turbulent state through the remainder of the expansion. As the strength of expansion increases because of either increasing Mach number or decreasing cone angle, the size of the distributed roughness (or the Reynolds number) must increase for effective tripping. Note, for instance in Fig. 16, that the expansion is substantially stonger at $M_\infty = 12.7$ than at $M_\infty = 8$.

The distributed roughness trip heights used in this current study varied from 8 to 25 mils. As previously stated, the 8-mil roughness proved to be ineffective at the Reynolds numbers encountered in these tests. Hence, for the case of VKF Tunnel B or VKF Tunnel F at $M_\infty \approx 12.5$, roughnesses on the order of 14 to 25 mils are required. The grit blasting technique consisted of air blasting hardened steel particles onto the model surface to roughen it. To date, this technique has produced a surface roughness up to 6 mils. Attempts to achieve larger roughnesses via larger particles, model material variations, and higher air delivery pressures have been unsuccessful. Therefore, the experimentalist should consider distributed roughness produced by grit blasting only if the required trip height, k, is equal to or less than 6 mils.

Evidence that distributed roughness trips produce relatively small disturbances (shock waves) in the flow field compared to equally effective spherical trips is demonstrated by the shadowgraph photographs of Fig. 17. Here, 14-mil applied grit and 4 δ_k^* high (0.63 in.) spherical trips are compared at identical test conditions. A series of shock waves emanating from the grit is barely visible in the upper photograph, and they are relatively weak in comparison to the shock wave produced by the spheres. One should recall that the distributed roughnesses applied for tripping purposes here are comparable to the roughness encountered on some flight vehicles. The roughness of actual flight vehicles varies substantially, depending upon the nosetip material used. However, for some materials, distributed roughness actually provides a better simulation of flight hardware than would a smooth surface model. A complete listing of all experimental data is included in Appendix A.

6.0 CONCLUSIONS

Research directed at establishing criteria for distributed roughness-type boundary-layer trips has been conducted and the following conclusions may be drawn from this work:

1. Sharp cone untripped (natural) transition data from the present results compare very well with Pate's correlation and lend credibility to the blunt nose results.

2. Single rows of spherical trips should be placed slightly forward of the "pressure distribution bucket" and should be from 2 δ_k^* to 4 δ_k^* high for effective trippping. The 4 δ_k^* value brings transition near the trip.

3. Triple rows of 2 δ_k^* high spherical trips perform as well as a single row of 4 δ_k^* high trips.

4. Spherical trip results on blunt-slender cones are in fair agreement with the Potter-Whitfield prediction technique.

5. Distributed roughness trips one-fifth the height of spherical trips yield excellent results while producing substantially less disturbance to the flow field as determined by shadowgraph photographs.

6. Distributed roughness applications on blunt-slender cones should start 45 deg off of the stagnation point and extend up to the "pressure bucket", or as close to it as practical.

7. As with spherical-type trips, the distributed roughness-type trip effectiveness is a strong function of Mach number.

8. The conical section of a roughened sphere-cone nose is more influential in determining trip effectiveness than is the spherical portion on an r_n= 0.589-in. nose.

9. The distributed roughness tripping elements in the forward section of a roughened nose evidently trip the boundary layer because of their relatively high value of k/δ_k^*, and, thereafter, the relatively small roughness maintains the turbulent state through the remainder of the expansion.

10. Distributed roughness element heights must increase as Mach number increases or cone angle decreases in order to maintain effective tripping.

REFERENCES

1. Whitfield, Jack D. and Dougherty, N. Sam, Jr. "A Survey of Transition Research at AEDC." AEDC-TR-77-52 (ADA041740), July 1977.

2. Potter, J. L. and Whitfield, J. D. "Effects of Slight Nose Bluntness and Roughness on Boundary Layer Transition in Supersonic Flows." Journal of Fluid Mechanics, Part IV, Vol. 12, 1962, pp. 501-535.

3. Sterrett, James R., Morrisette, E. Leon, Whitehead, Allen H., Jr., and Hicks, Raymond M. "Transition Fixing for Hypersonic Flow." NASA TN D-4129, October 1967.

4. Pate, S. R. "Supersonic Boundary Layer Transition: Effects of Roughness and Freestream Disturbances." AIAA Journal,Vol. 9, No. 5, May 1971, pp. 797-803.

5. Pate, S. R. "Dominance of Radiated Aerodynamic Noise on Boundary-Layer Transition in Supersonic-Hypersonic Wind Tunnels: Theory and Application." Ph.D. Dissertation, The University of Tennessee, Knoxville, Tenn., March 1977.

6. Test Facilities Handbook (Tenth Edition). "von Kármán Gas Dynamics Facility, Vol. 3." Arnold Engineering Development Center, May 1974.

7. Pate, S. R. and Eaves, R. H., Jr. "Recent Advances in the Performance and Testing Capabilities of the AEDC-VKF Tunnel F (HOTSHOT) Hypersonic Facility." AIAA Paper No. 74-84, Presented at the AIAA 12th Aerospace Sciences Meeting, Washington, D. C., January 30 - February 1, 1974.

8. Ledford, R. L., Smotherman, W. E., and Kidd, C. T. "Recent Developments in Heat-Transfer-Rate, Pressure, and Force Measurements for Hotshot Tunnels." AEDC-TR-66-228 (AD645764), January 1967.

9. Bynum, D. S. "Instrumentation for the AEDC/VKF 100-in. Hotshot (Tunnel F)." AEDC-TR-66-209 (AD804567), January 1967.

10. Fay, J. A. and Riddell, F. R. "Theory of Stagnation Point Heat Transfer in Dissociated Air." Journal of the Aeronautical Sciences, Vol. 25, No. 2, February 1958, pp. 73-85, 121.

11. Brahinsky, Herbert, S. and Neal, Charles A. "Tables of Equilibrium Thermodynamic Properties of Nitrogen." Vol. I-IV, AEDC-TR-69-126, August 1969.

12. Griffith, B. J. and Lewis, Clark H. "Laminar Heat Transfer to Spherically Blunted Cones at Hypersonic Conditions." AIAA Journal, Vol. 2, No. 3, March 1964, pp. 438-444.

13. Grabau, Martin, Smithson, H. K., Jr., and Little, W. J. "A Data Reduction Program for Hotshot Tunnels Based on the Fay-Riddell Heat-Transfer Rate Using Nitrogen at Stagnation Temperatures from 1500°K to 5000°K." AEDC-TR-64-50 (AD601070), June 1964.

14. Van Driest, E. R. and Blumer, C. B. "Boundary Layer Transition on Cones and Spheres at Supersonic Speeds-Effects of Roughness and Cooling." AFOSR Scientific Report No. 67-2048, Ocean Systems Operations of North American Rockwell Corporation, Anaheim, California, July 1967.

15. Demetriades, A. "Hydrodynamic Stability and Transition to Turbulence in the Hypersonic Boundary Layer Over a Sharp Cone." AFOSR-TR-75-1435 (ADA016536), July 1975.

16. Mayne, A. W., Jr. and Dyer, D. F. "Comparison of Theory and Experiment for Turbulent Boundary Layers on Simple Shapes at Hypersonic Conditions." Proceedings of the 1970 Heat-Transfer and Fluid Mechanics Institute, Stanford University Press, 1970, pp. 168-188.

17. Pate, S. R. "Measurements and Correlations of Transition Reynolds Numbers on Sharp Slender Cones at High Speeds." AEDC-TR-69-172 (AD698326), also AIAA Journal, Vol 9, No. 6, June 1971, pp. 1082-1090.

18. Stainback, P. Calvin. "Effect of Unit Reynolds Number, Nose Bluntness, Angle of Attack, and Roughness on Transition on a 5° Half-Angle Cone at Mach 8." NASA TN D-4961, January 1969.

19. Potter, J. Leith and Whitfield, Jack D. "Boundary-Layer Transition Under Hypersonic Conditions." AEDC-TR-65-99 (AD462716), May 1965, Presented at AGARD Specialists' Meeting on "Recent Developments in Boundary Layer Research", Naples, Italy, AGARDograph 97, Part III, May 1965.

20. Coats, Jack D. "Investigation of the Effects of Nose Bluntness on Natural and Induced Boundary-Layer Transition on Axisymmetric Bodies in Supersonic Flow." AEDC-TR-73-36 (AD755843), February 1973.

21. Launder, B. E. and Jones, W. P. "On the Prediction of Laminarization." Ministry of Technology Aeronautical Research Council, C. P. No. 1036, 1968.

22. McCauley, W. D., Saydah, A., and Bueche, J. "The Effect of Controlled Three Dimensional Roughness on Hypersonic Laminar Boundary Layer Transition." AIAA Paper 66-26, January 1966.

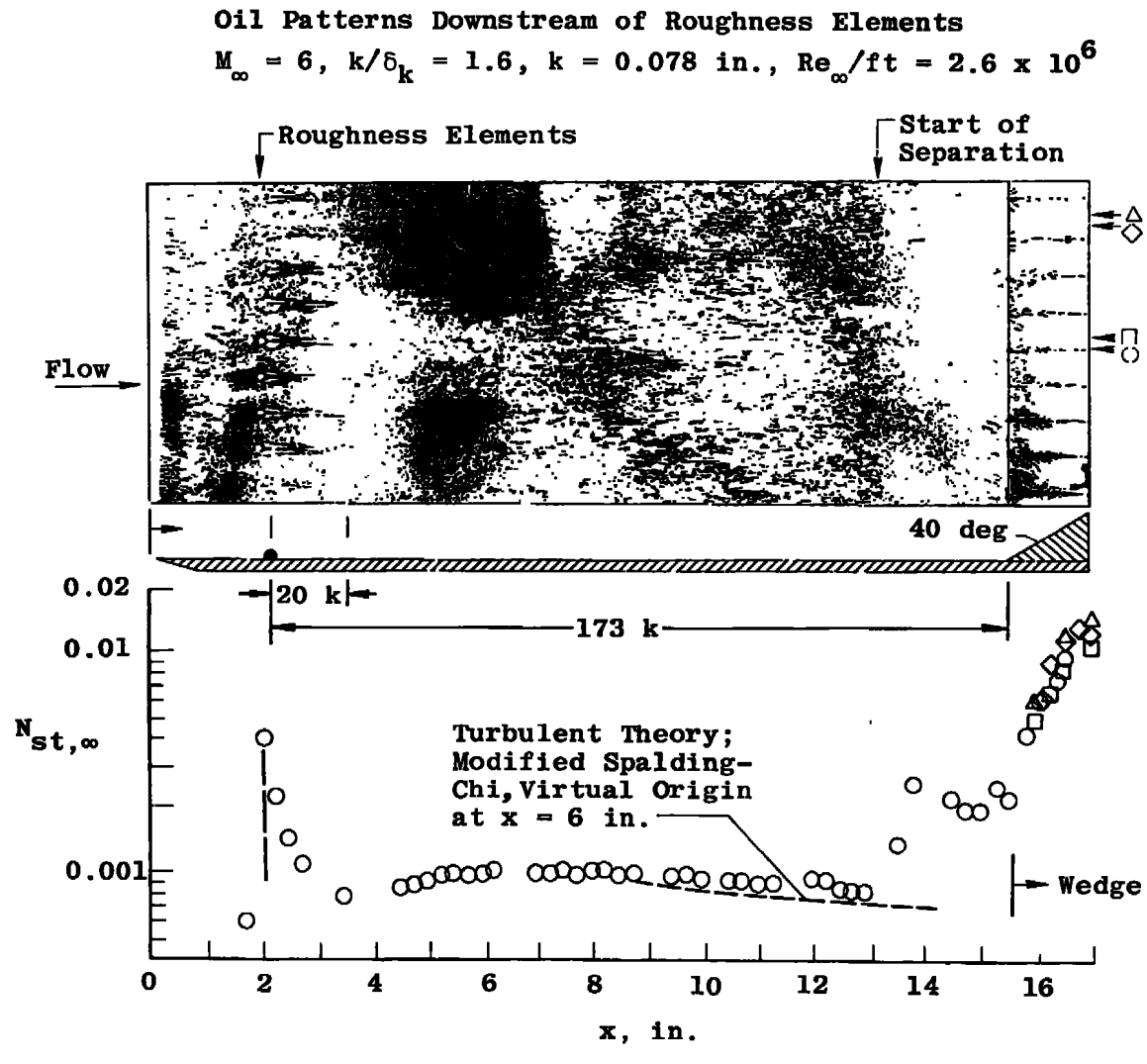

Figure 1. Downstream disturbances as reported by Sterrett et al., Ref. 3.

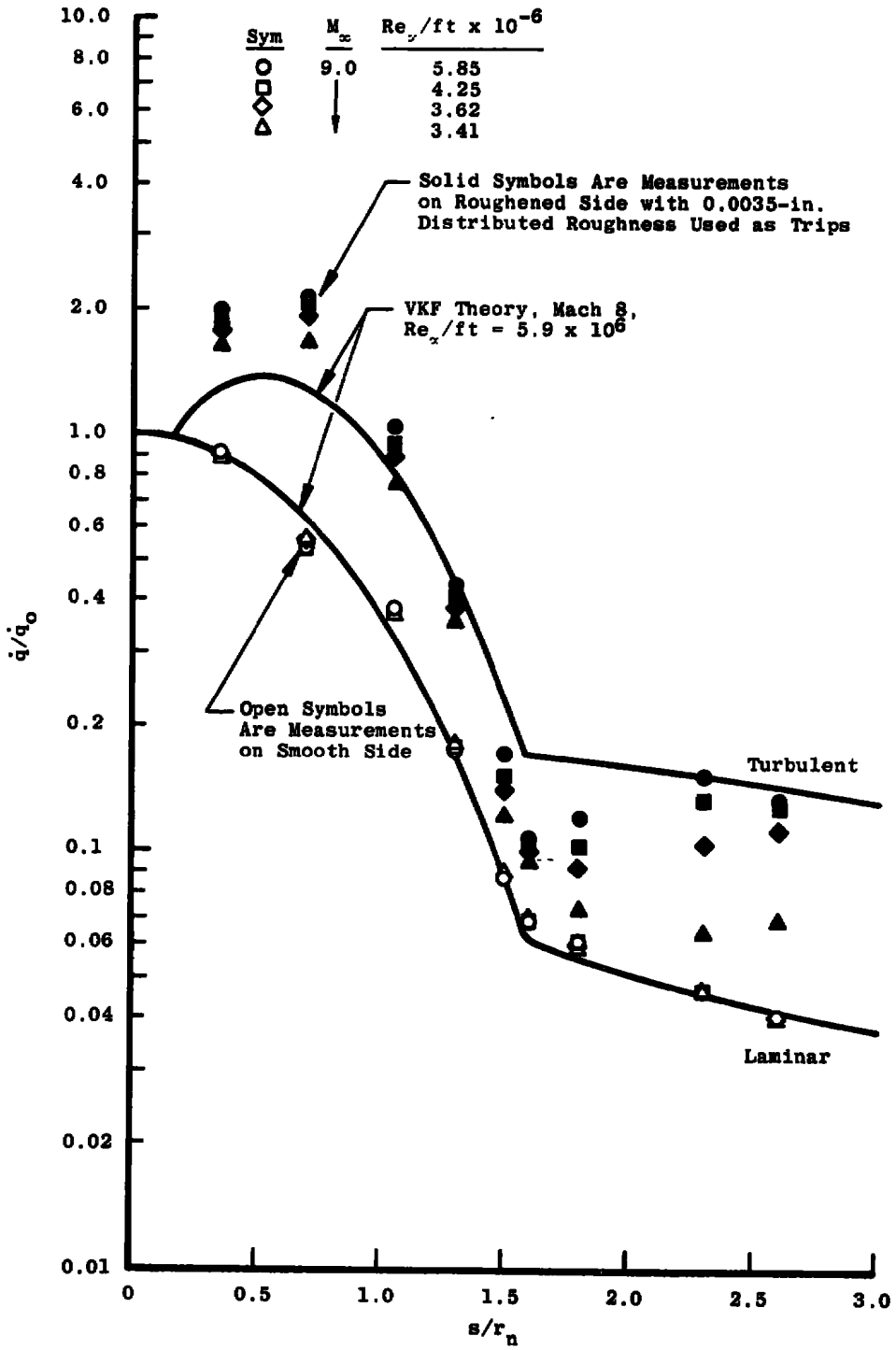

Figure 2. Measured heat-transfer distribution on a 5-in.-diam hemisphere cylinder at Mach 9.

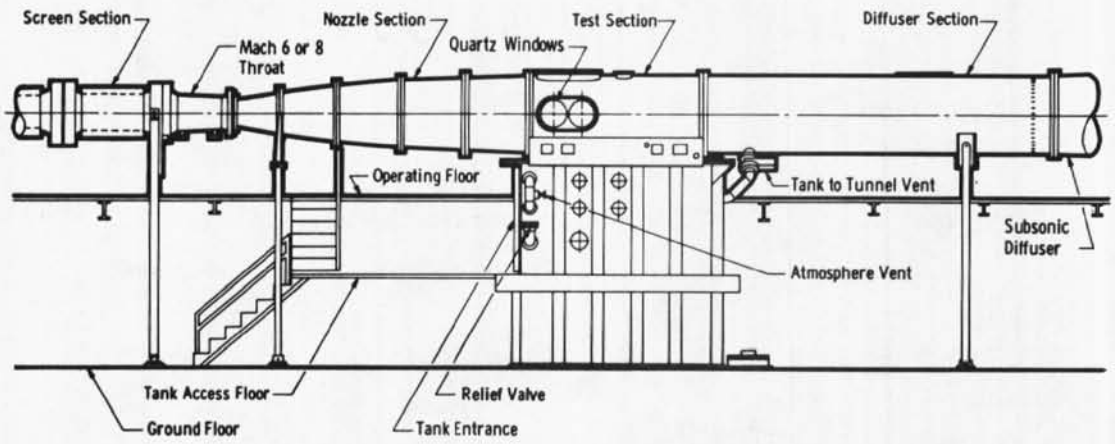

a. Tunnel assembly

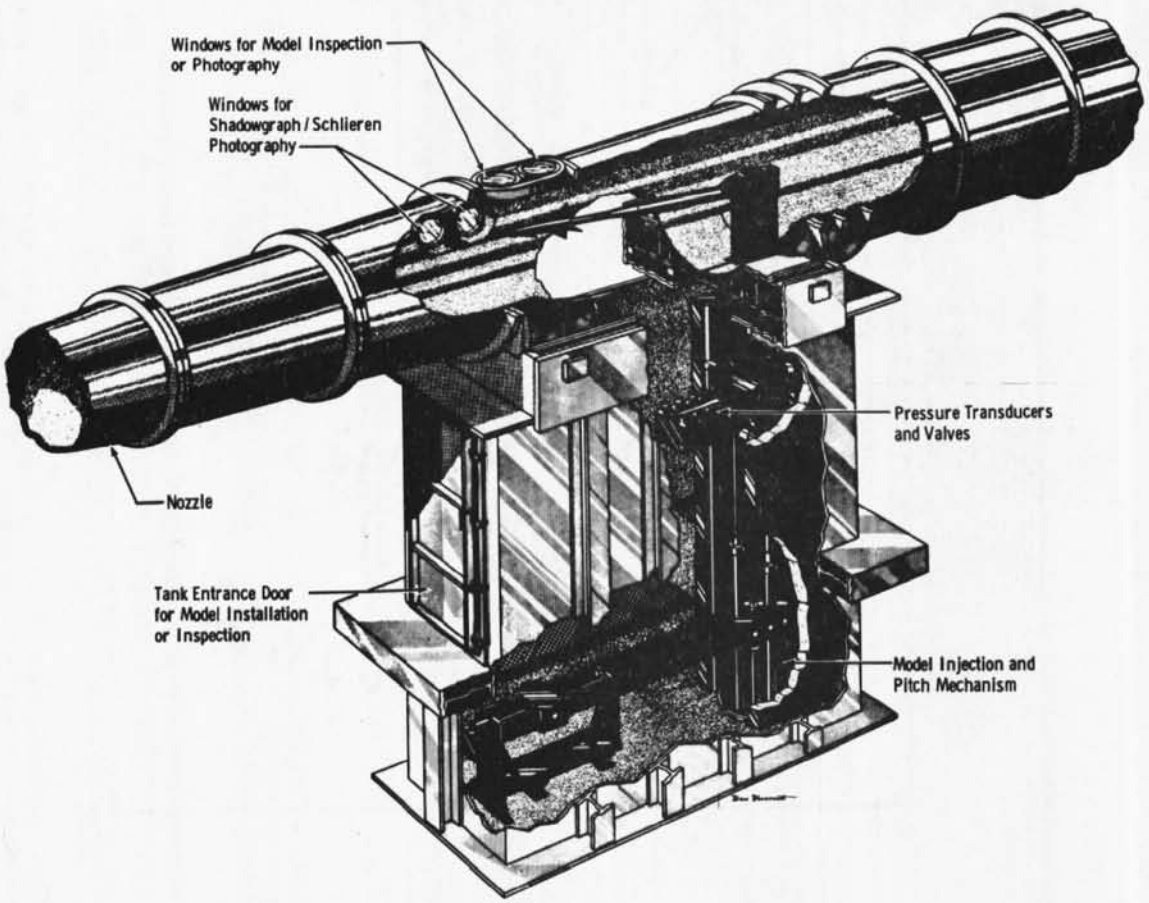

b. Tunnel test section

Figure 3. AEDC-VKF Tunnel B.

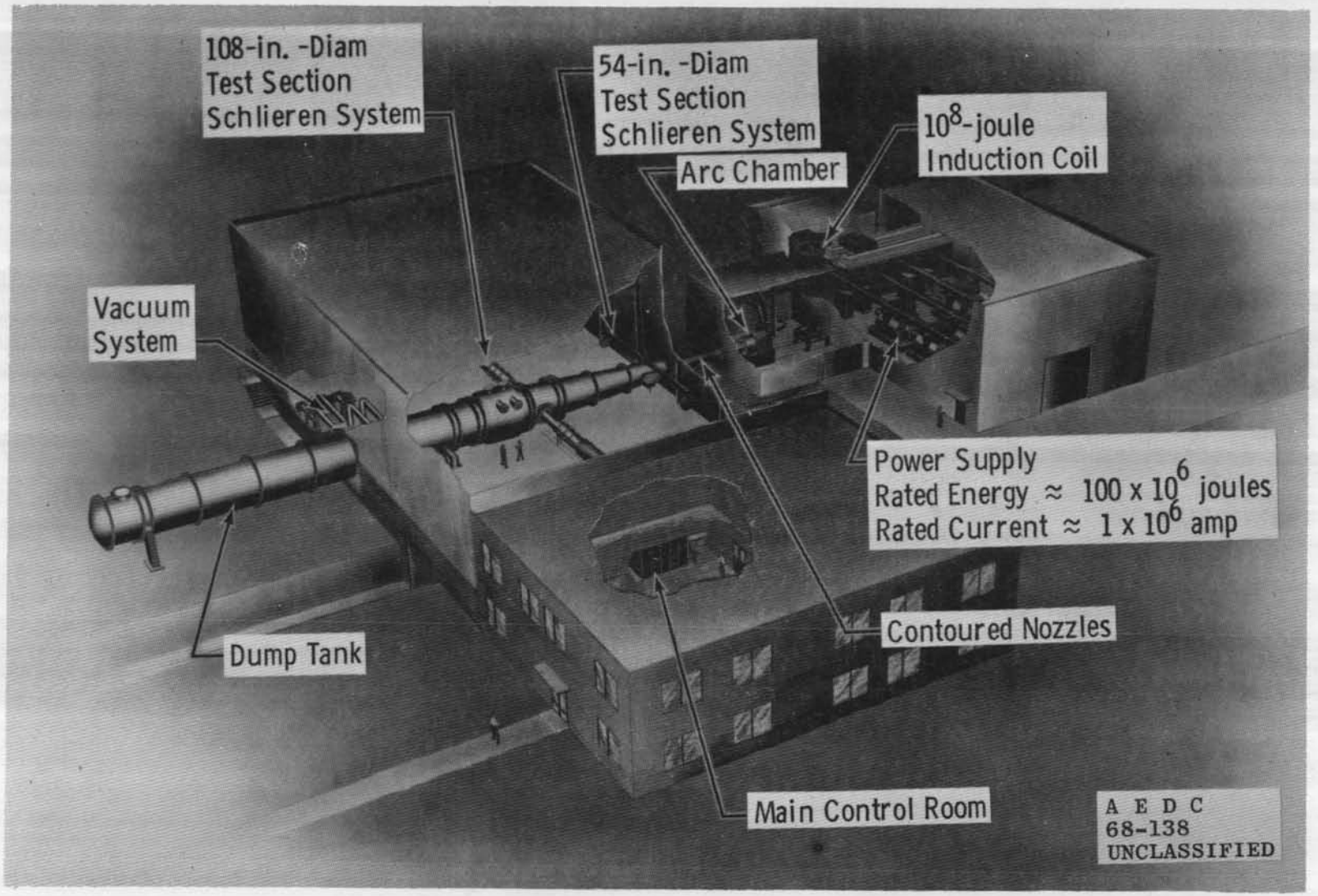

Figure 4. AEDC-VKF Tunnel F plant.

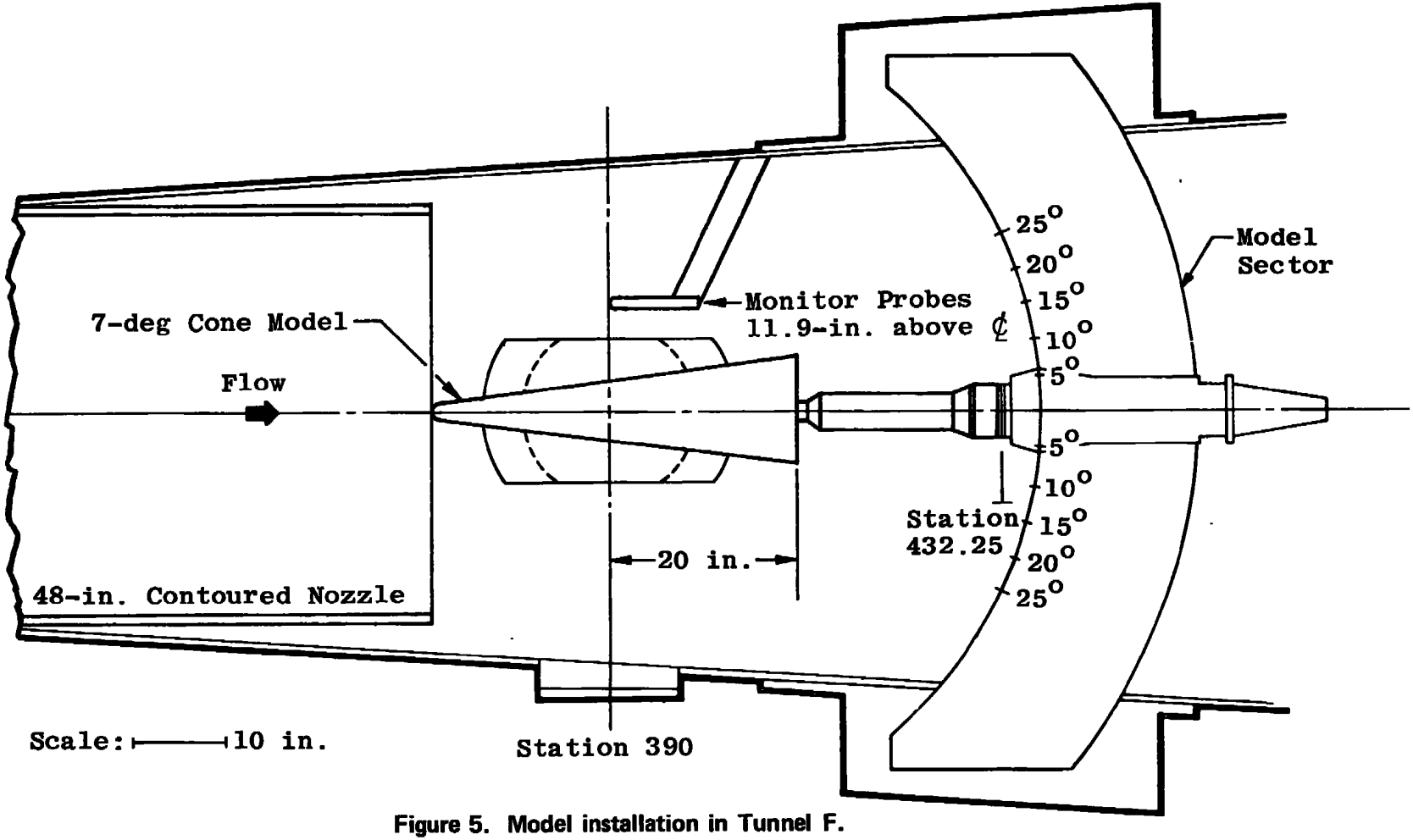

Figure 5. Model installation in Tunnel F.

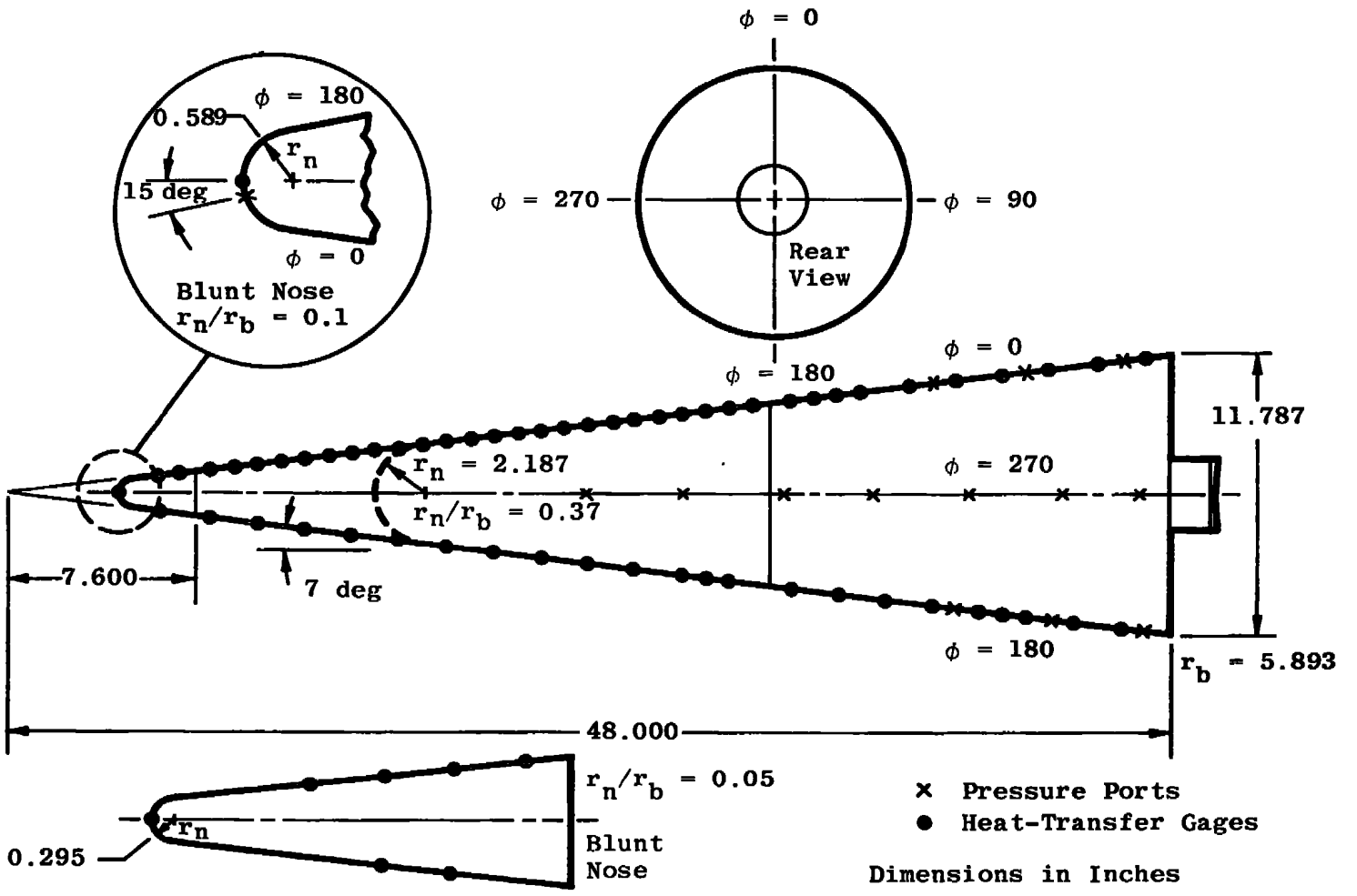

Figure 6. Pressure/heat-transfer model (7-deg cone).

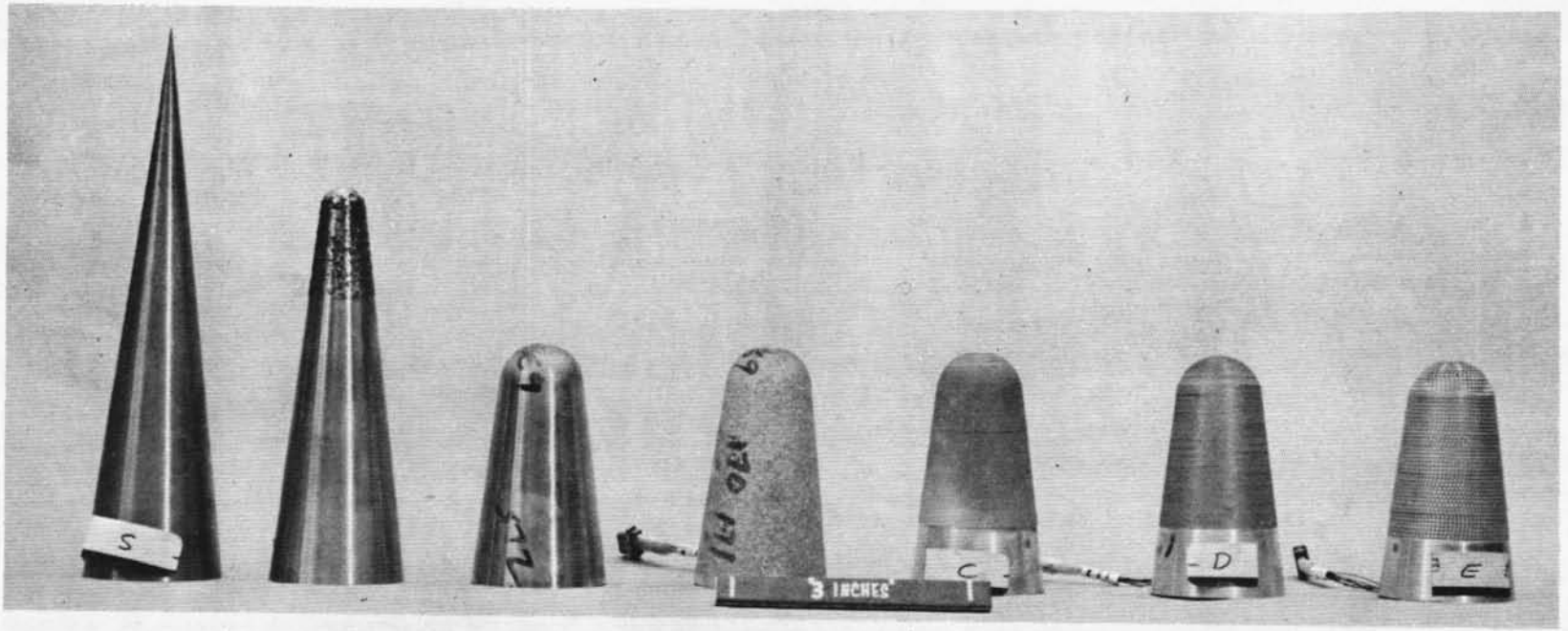

Sharp Nose	r_n = 0.295-in. Nose with 10-mil Grit Applied	Smooth, r_n = 0.589 in.	r_n = 0.589-in. Nose, Grit Blasted to 5-mil Roughness	r_n = 0.589-in. Nose, 8-mil NCM Roughness	r_n = 0.589-in. Nose, 14-mil NCM Roughness	r_n = 0.589-in. Nose, 25-mil NCM Roughness

a. Sharp, r_n = 0.295, and r_n = 0.589-in. noses

Figure 7. Photographs of 7-deg cone noses.

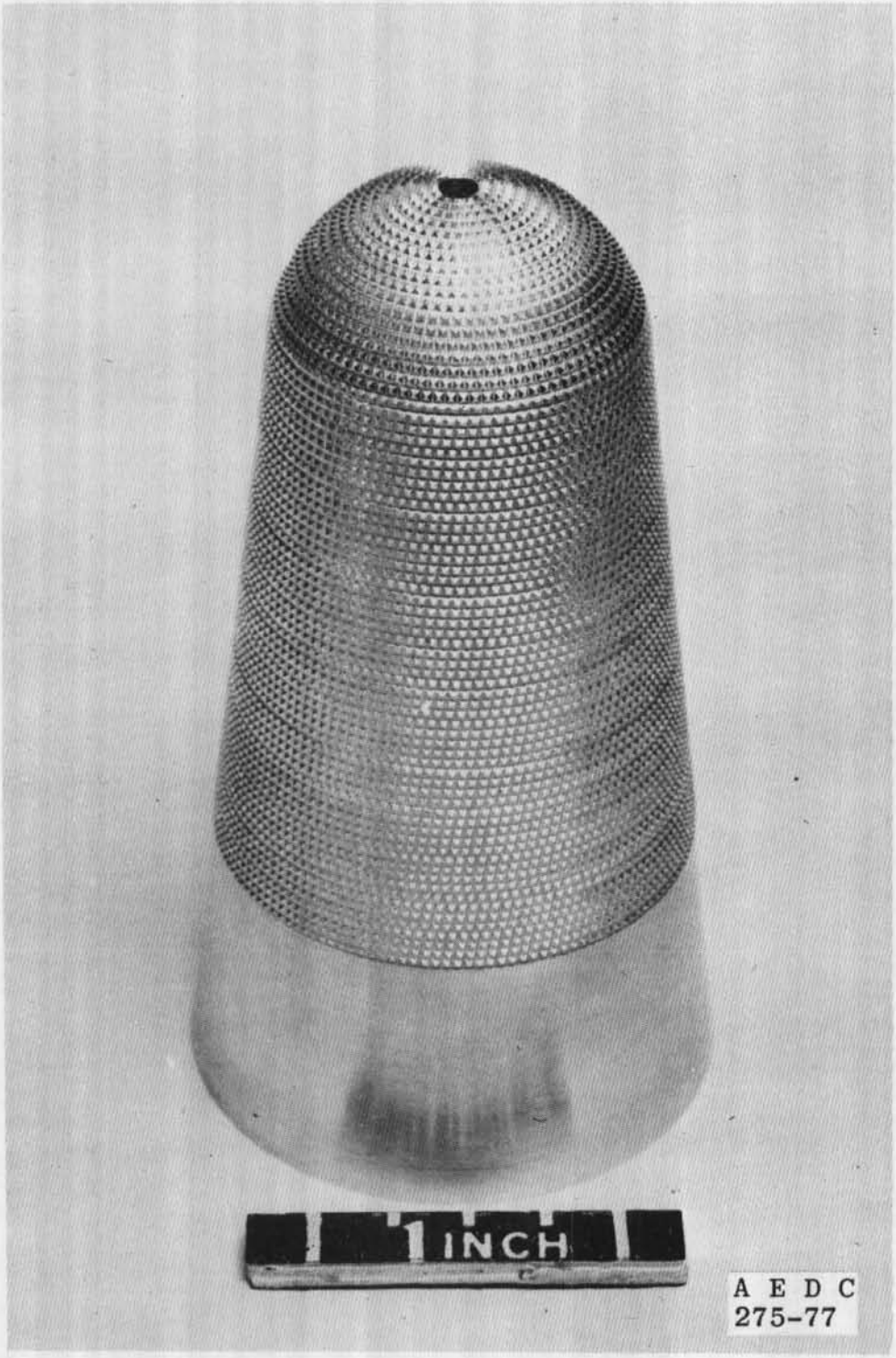

b. Blunt nose, r_n = 0.589 in., 25-mil NCM
Figure 7. Continued.

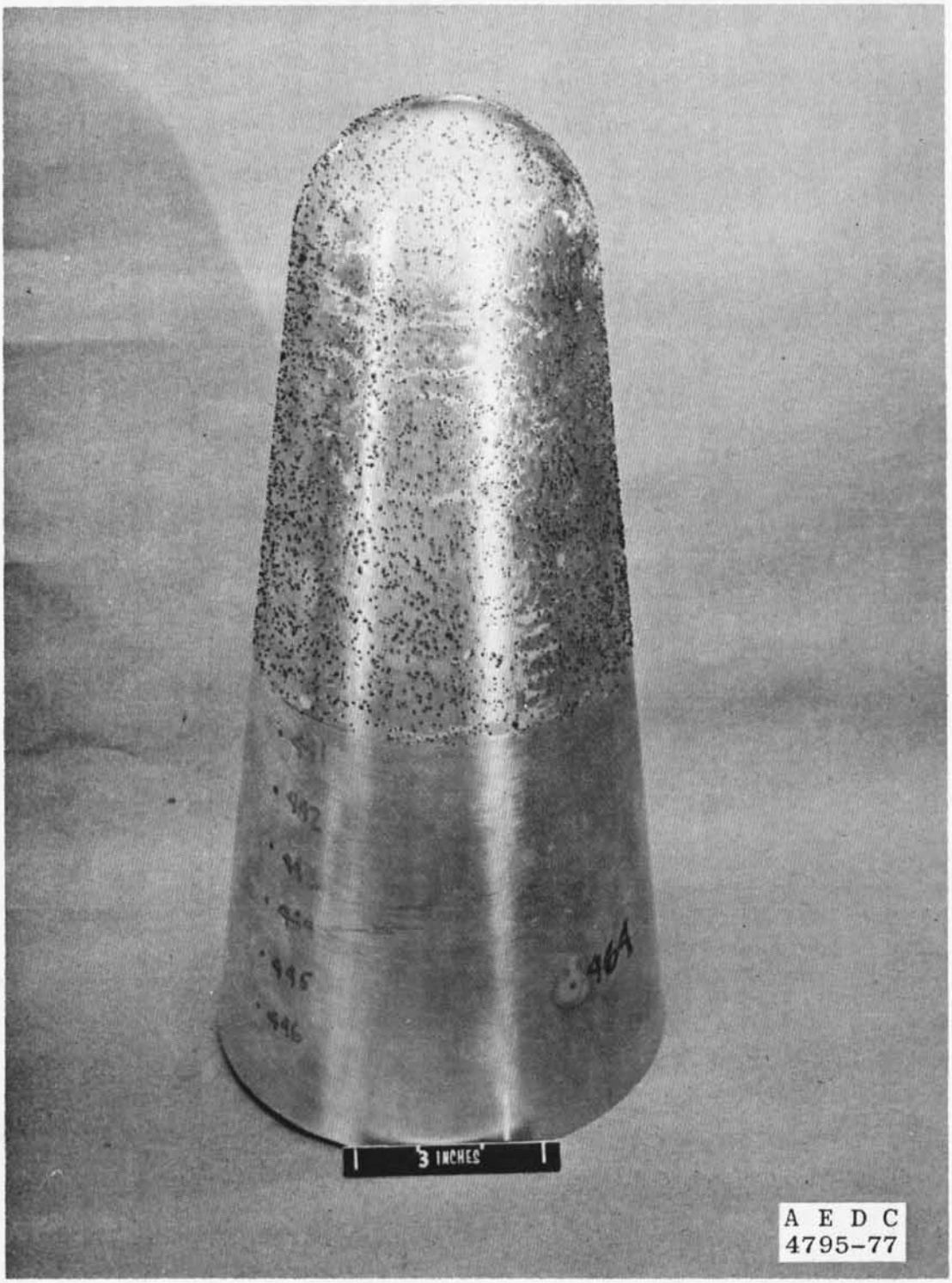

c. Blunt nose, r_n = 2.187 in., 25-mil grit
Figure 7. Concluded.

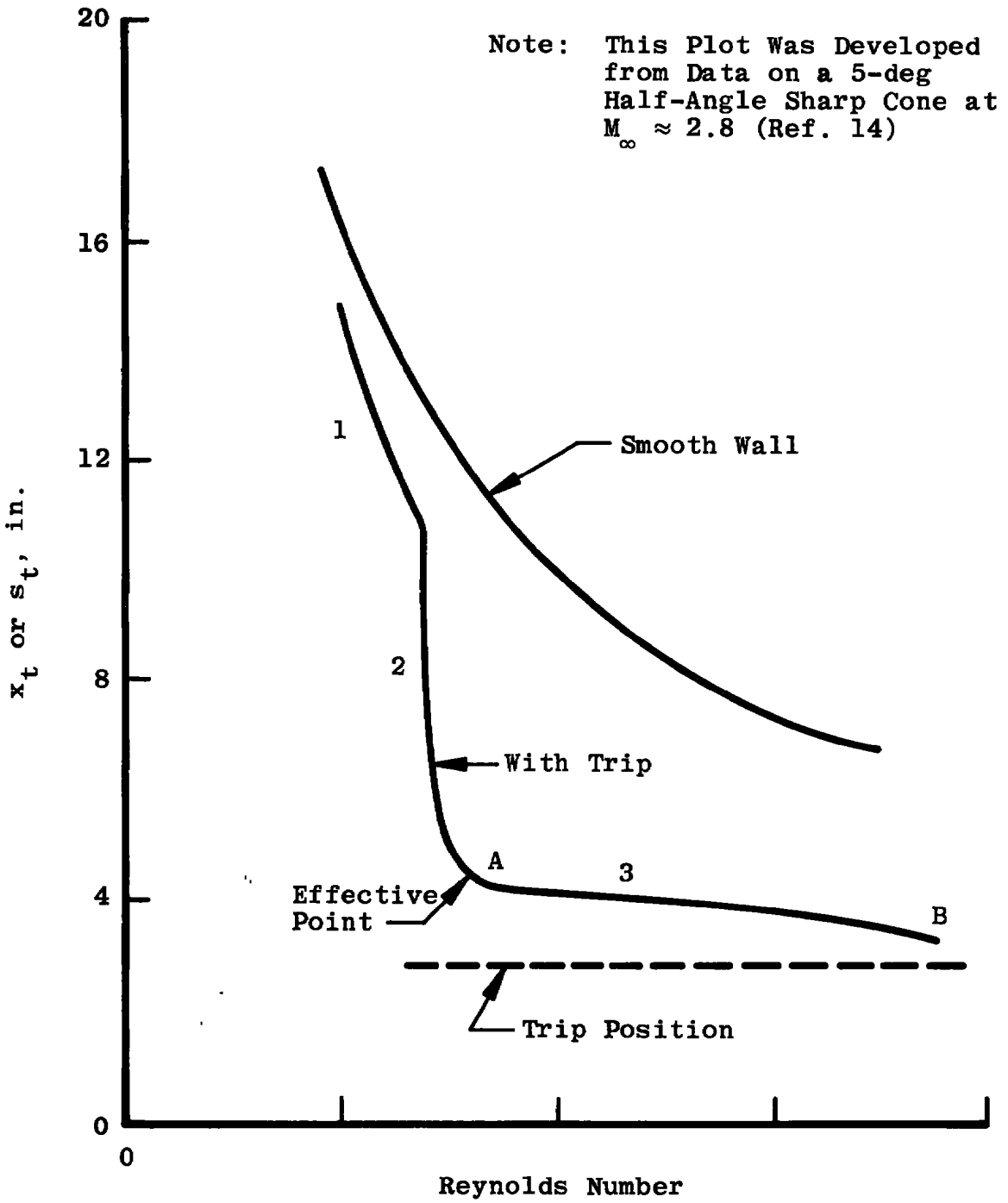

Figure 8. Variation of x_t with unit Reynolds number.

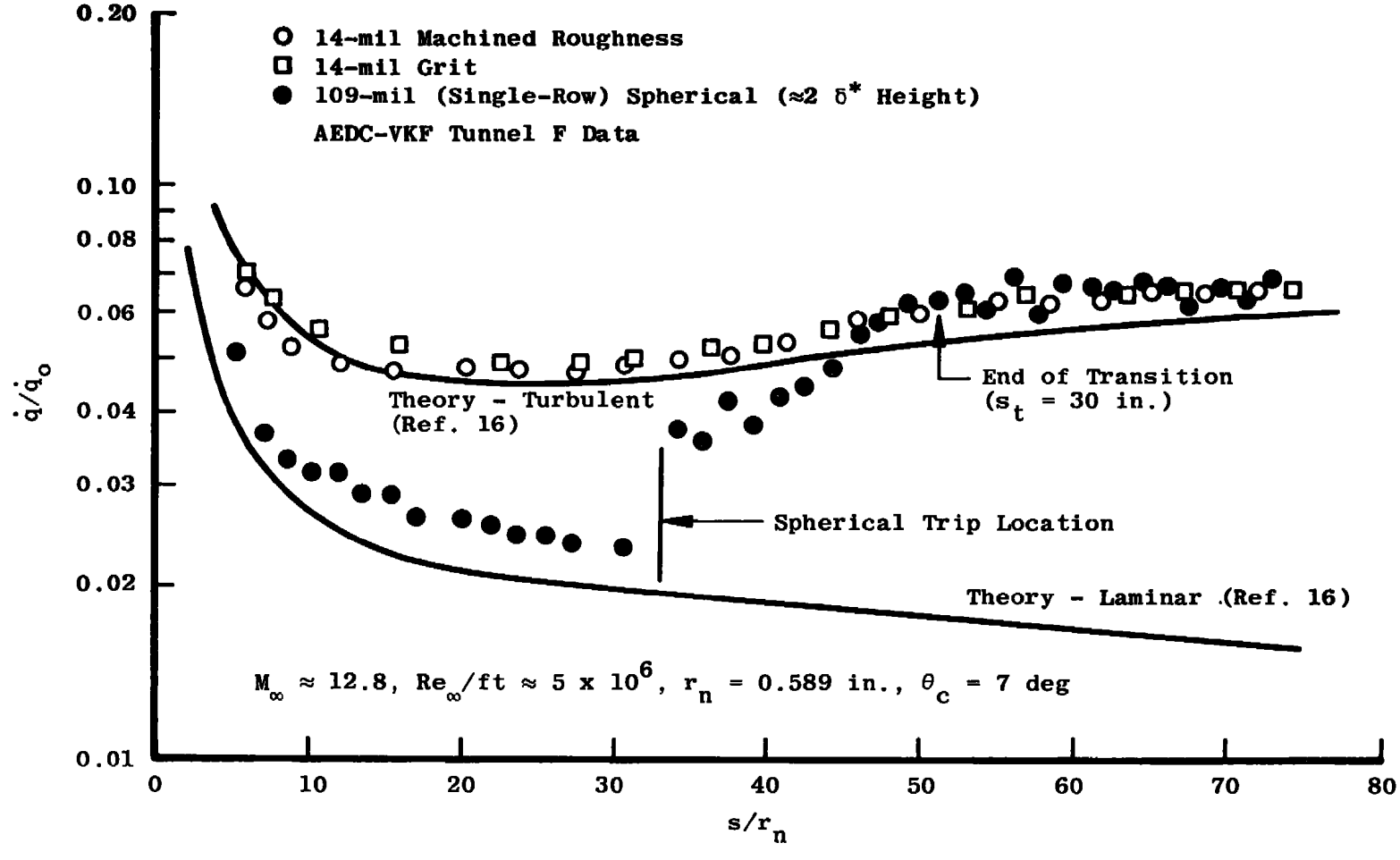

Figure 9. Comparison of heat-transfer distribution on blunt cone using distributed roughness and spherical trips.

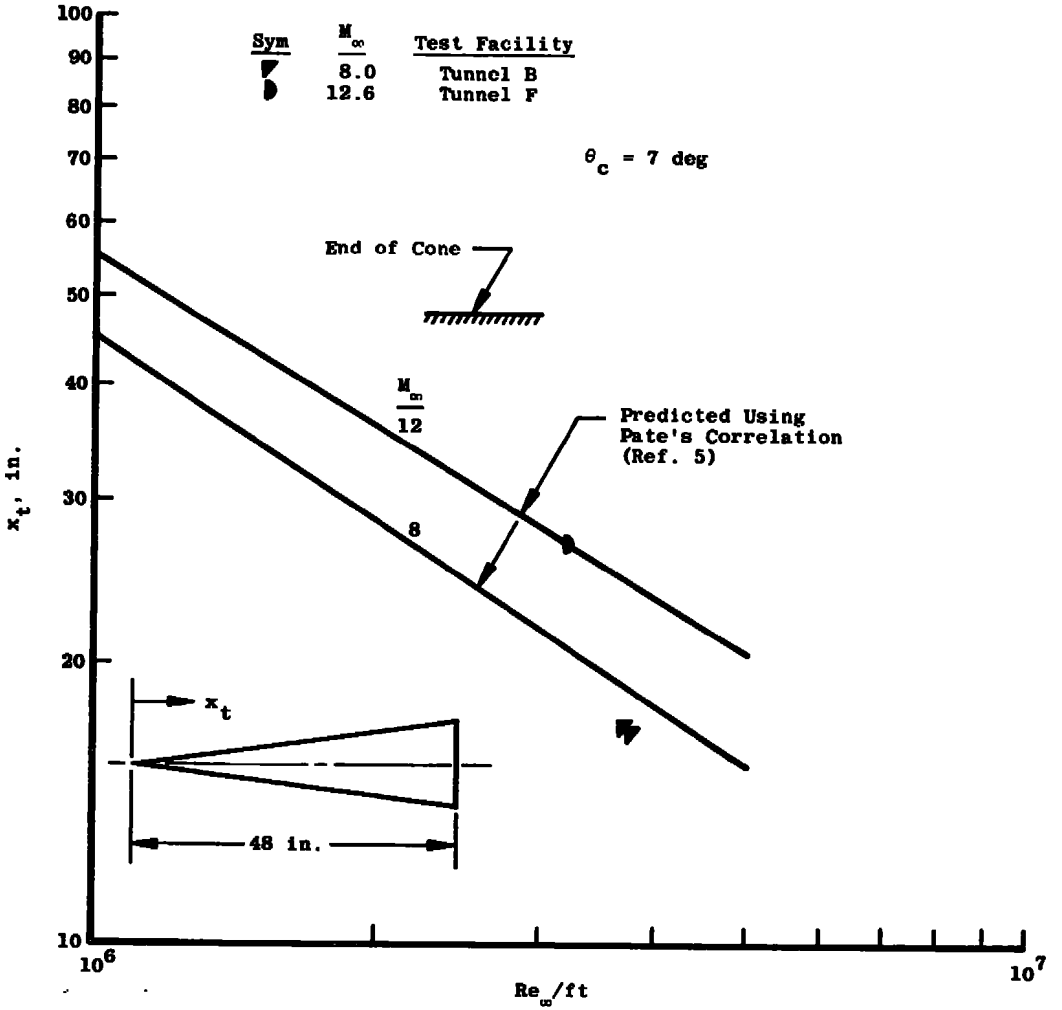

Figure 10. Sharp cone natural transition results compared to Pate's correlation prediction.

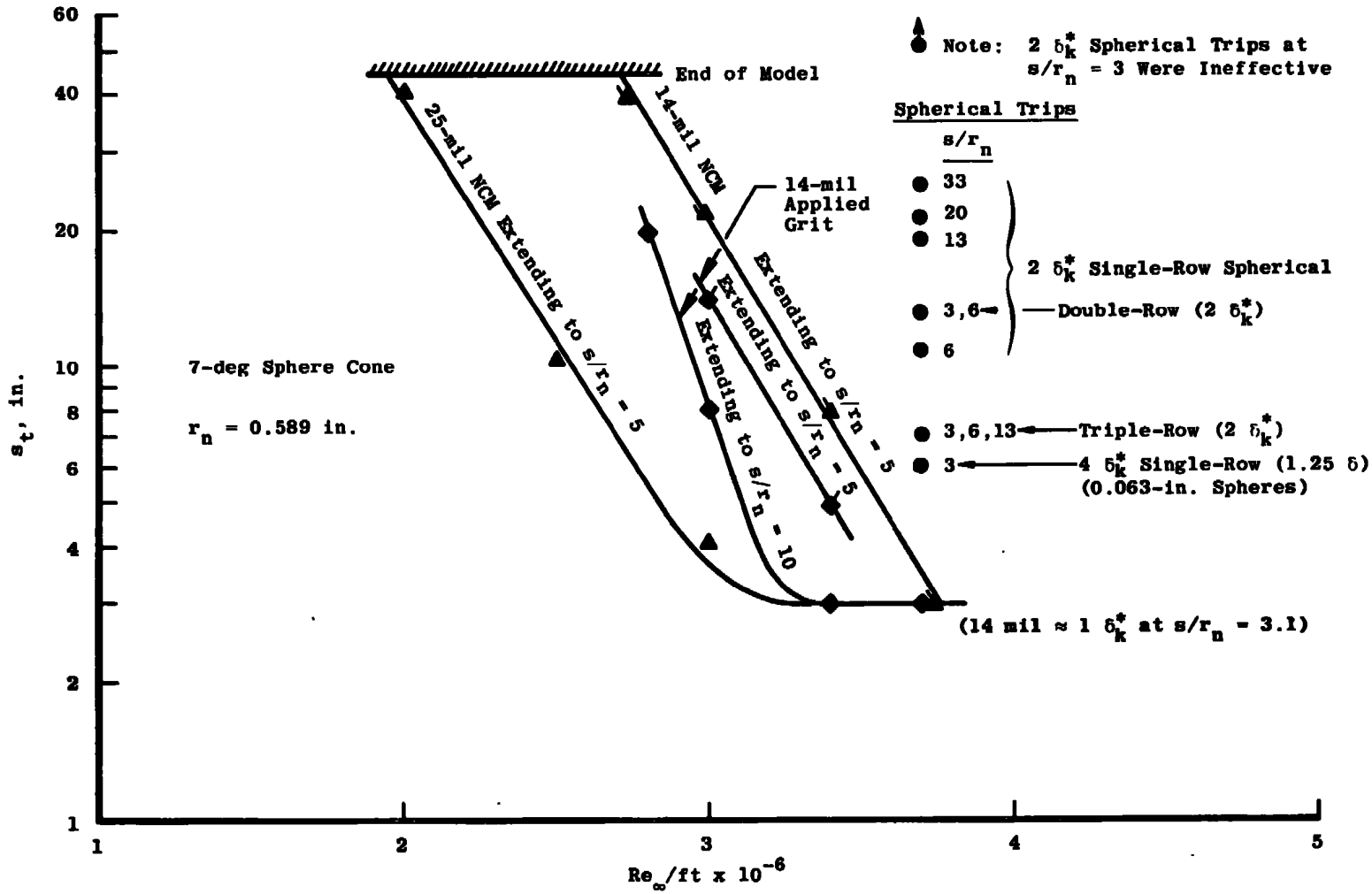

Figure 11. Comparison of distributed roughness and spherical trips at Mach 8.

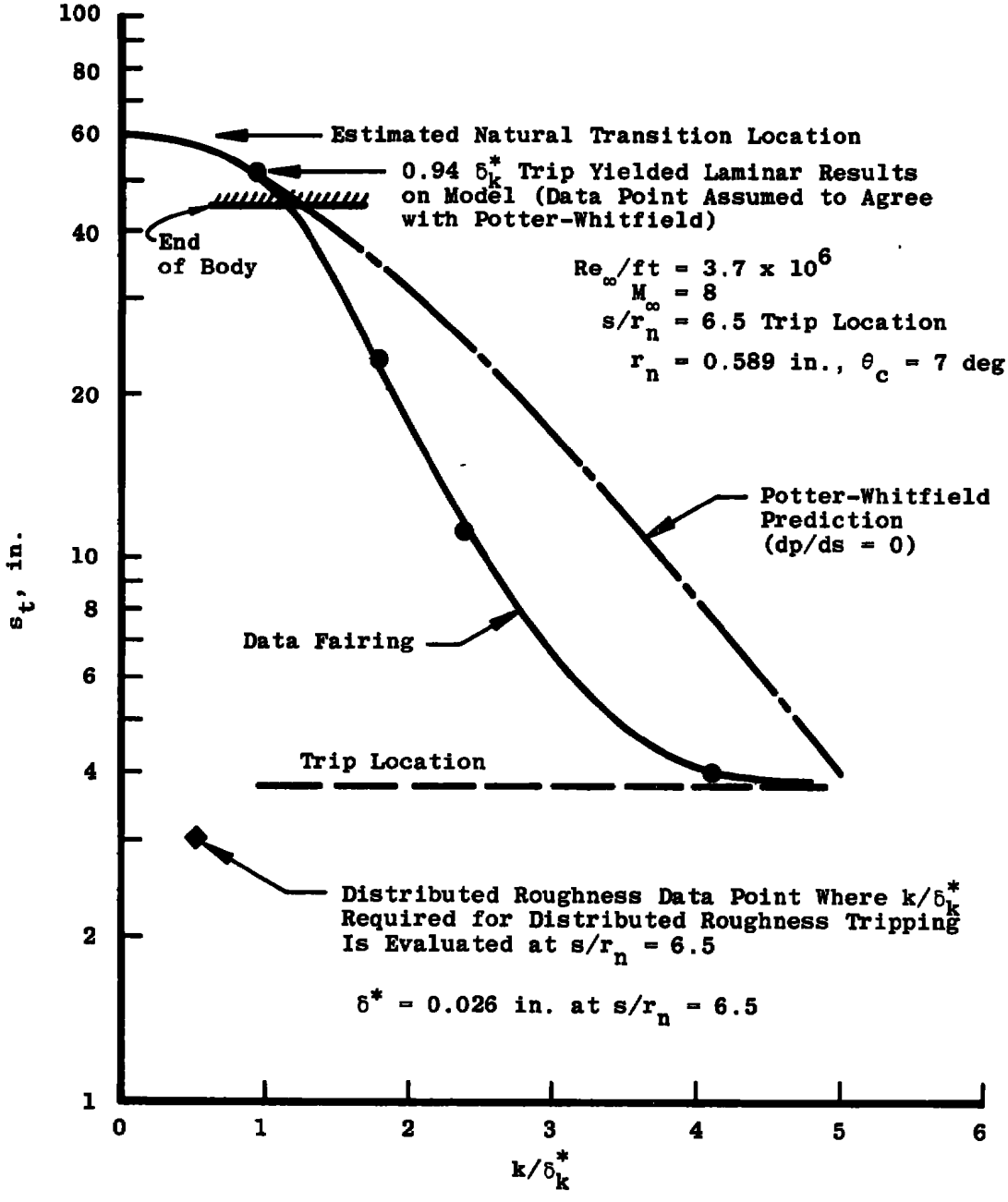

Figure 12. Single-row spherical trip results compared to the Potter-Whitfield prediction (Ref. 19).

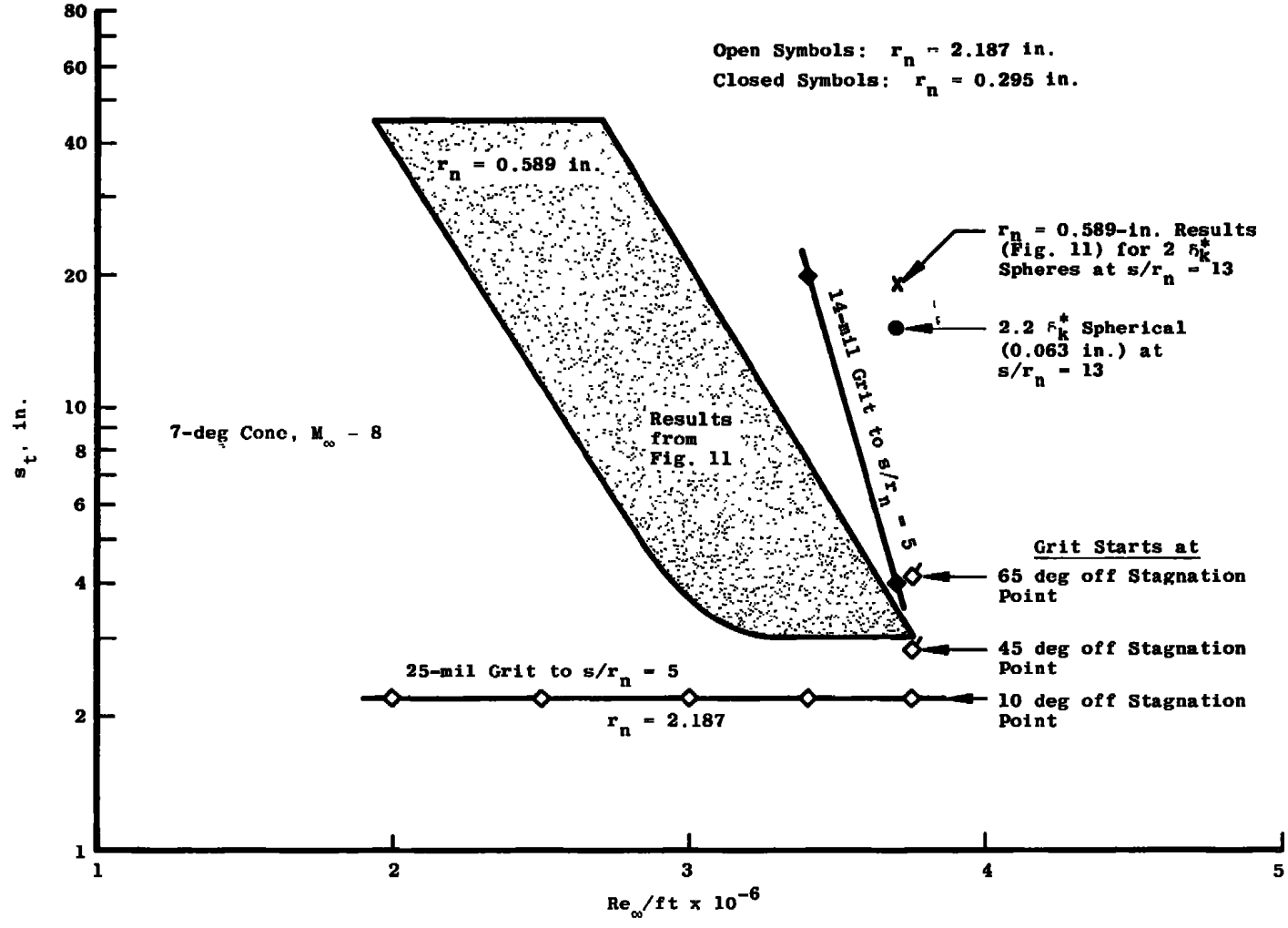

Figure 13. Tripped transition location data obtained on the r_n/r_b = 0.05 and 0.37 bluntness cone configuration at Mach 8.

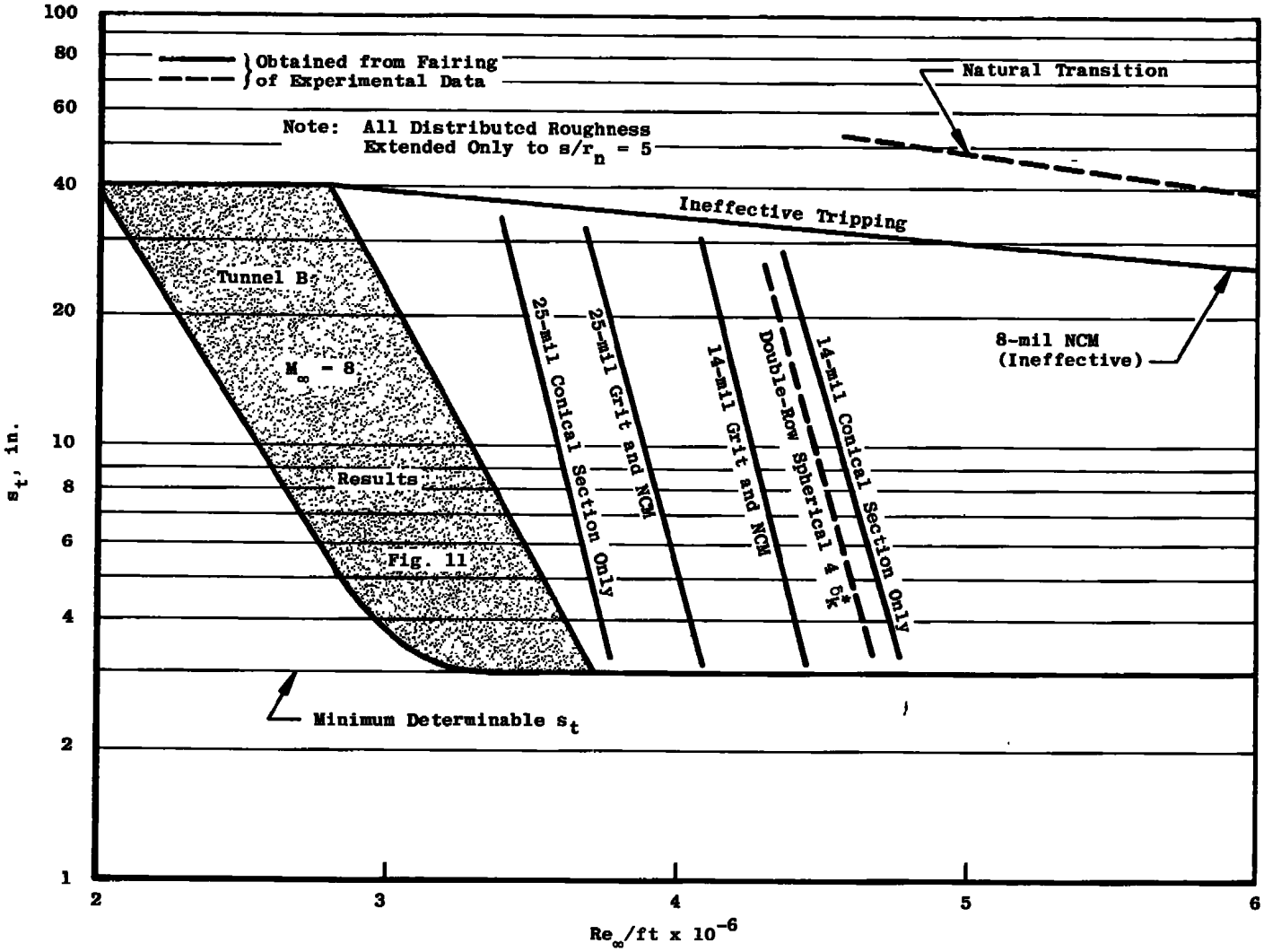

Figure 14. Summary of tripped results at $M_\infty \approx 12.7$; $r_n = 0.589$ in., 7-deg cone.

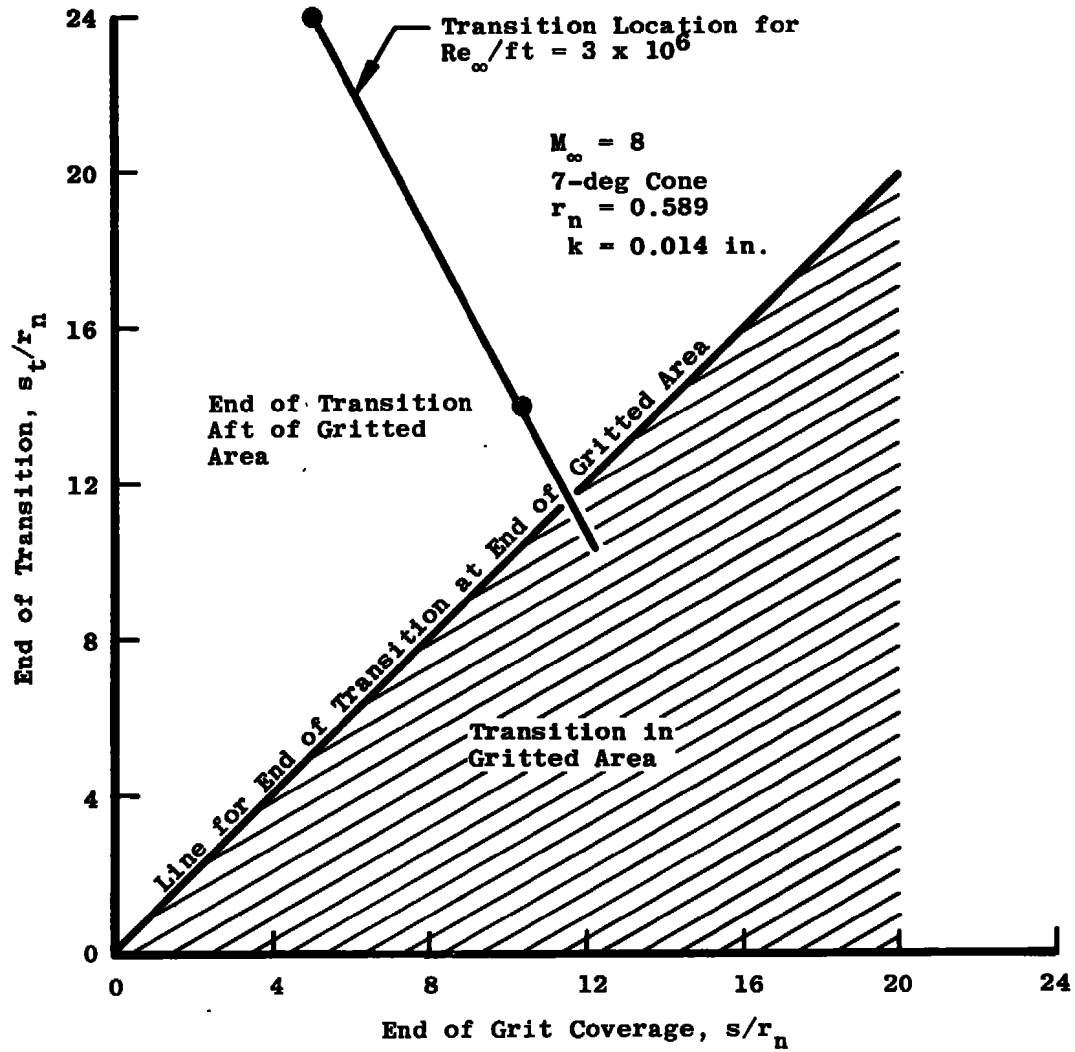

Figure 15. Influence of the extent of grit coverage on transition location.

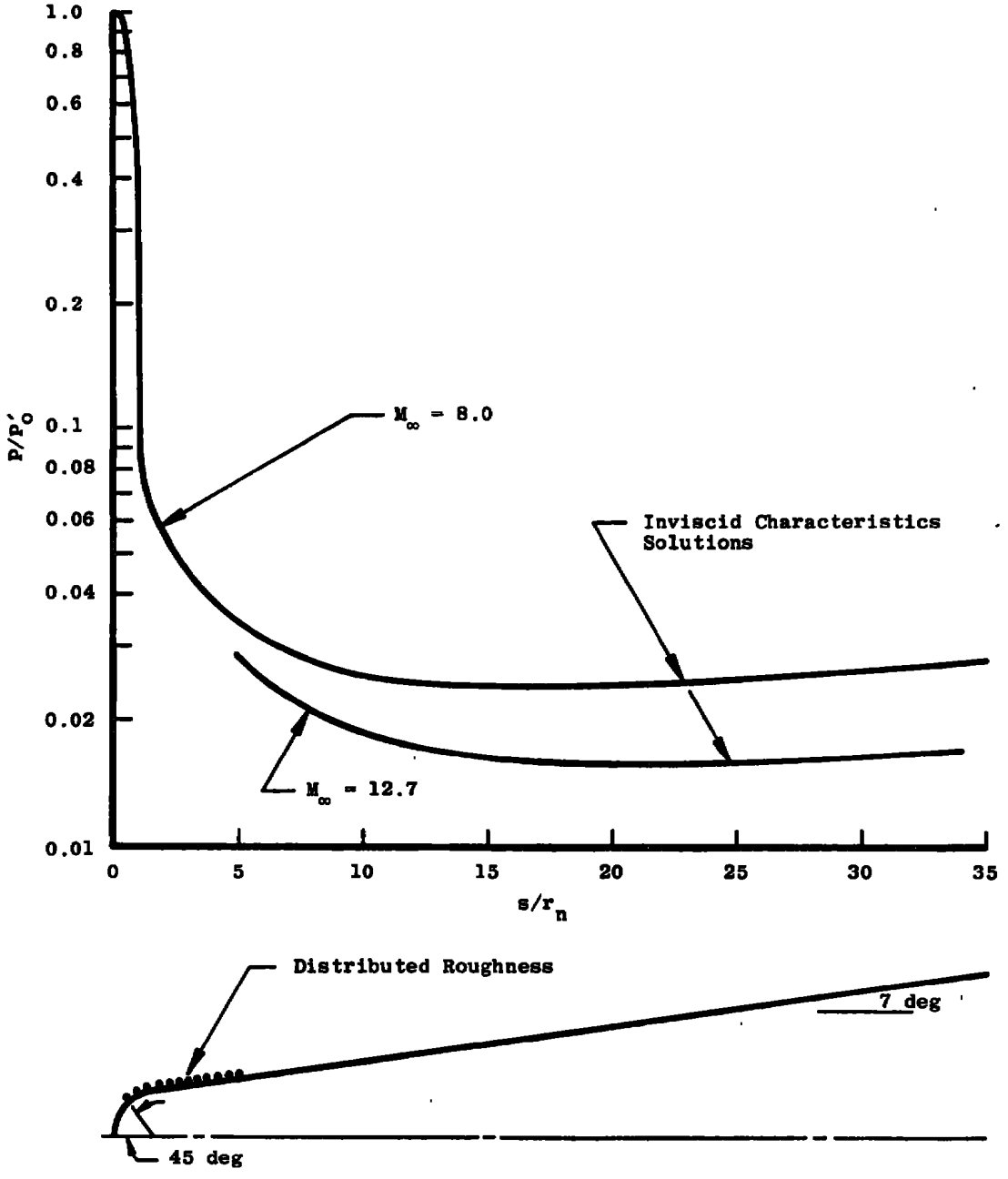

Figure 16. Pressure distribution on the 7-deg sphere cone.

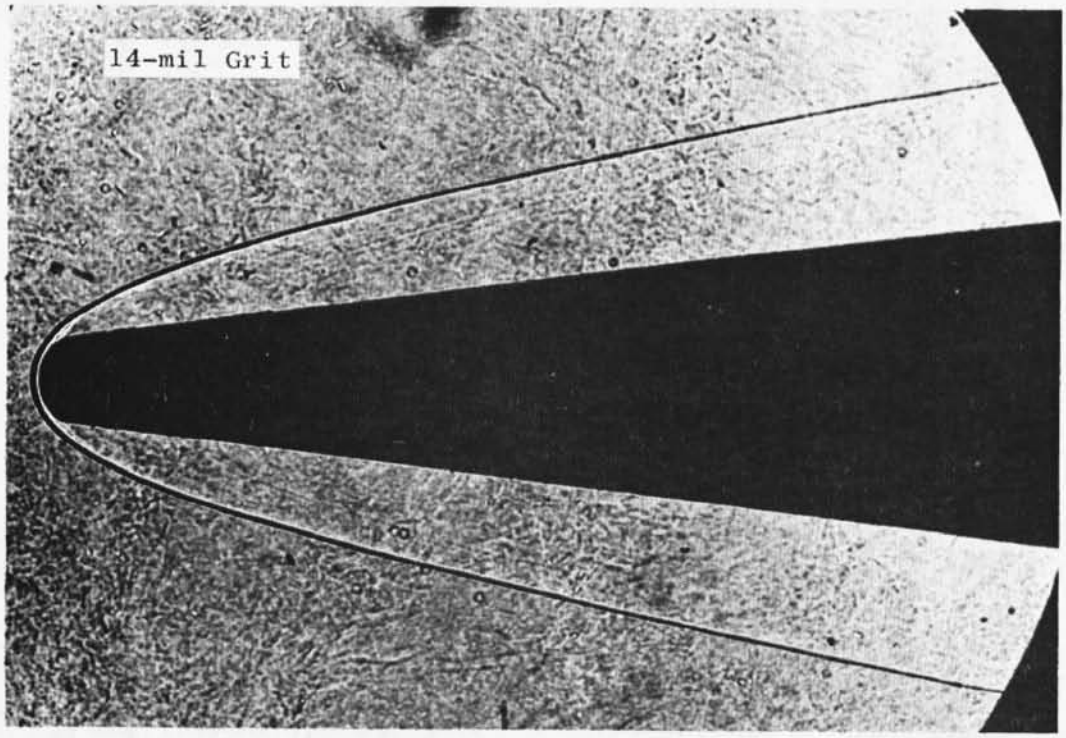

$M_\infty = 8$, $r_n = 0.589$ in., $Re_\infty/ft = 3.7 \times 10^6$

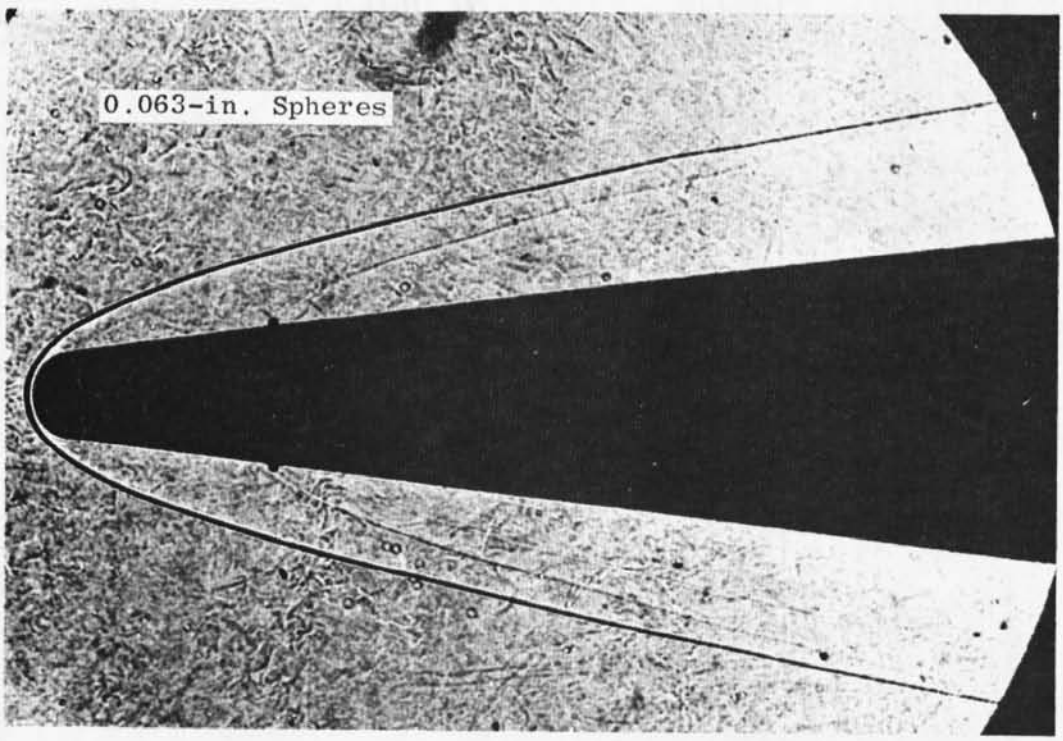

Figure 17. Shadowgraphs of trip-induced flow-field disturbances.

APPENDIX A
7-DEG CONE RESULTS

Tunnel	Data Group	M_∞	Re_∞/ft x 10^{-6}	r_n, in.	k, in.	Type Trip	Extent, s/r_n Range	s_t, in.
F	5686	12.5	6.27	0.589	0.008	NCM*	0.25-5.0	15
			5.92					28
			5.20					32
	5682	11.5	4.45	0.589	0.014	NCM	0.10-5.0	3
			4.00					30
	5690	12.3	5.86	0.589	0.014	NCM	0.10-5.0	3
			5.24					3
			4.78					29
			4.20					45
	5684	12.2	5.45	0.589	0.014	Distributed Grit	0.20-5.0	3
			4.89					3
			4.39					3
			4.13					28
			3.32					31
			3.07					40
	5685	12.6	4.81	0.589	0.014	Distributed Grit	0.20-1.5	29
			4.24					37
	5697	12.5	5.25	0.589	0.014	Distributed Grit	1.5-5.0	3
			4.78					3
			4.34					32
			3.92					38
			3.24					40
	5687	12.8	5.10	0.589	0.025	NCM	0.10-1.5	3
			4.27					3
			3.78					29
			3.45					33
			3.14					44

*Indicates Numerically Controlled Machine Roughness

Tunnel	Data Group	M_∞	$Re_\infty/ft \times 10^{-6}$	r_n, in.	k, in.	Type Trip	Extent, s/r_n Range	s_t, in.
F	5688	12.8	5.23	0.589	0.025	Distributed Grit	0.20-5.0	3
			4.17					3
			3.70					32
			3.15					40
	5699	11.5	4.27	0.589	0.025	Distributed Grit	1.5-5.0	3
			4.04					3
			3.77					3
	5689	12.5	5.09	0.589	0.025	Distributed Grit	1.5-5.0	3
			4.15					3
			3.69					5
			3.44					32
			3.12					38
	5691	11.0	6.32	0.589	0.025	1-Row Spheres	3.1	44
	5692	12.3	5.11	0.589	0.109	1-Row Spheres	33.0	29
			4.21					38
	5693	11.8	5.49	0.589	0.025 and 0.047	2-Row Spheres	3.1 and 6.5	26
			5.28					45
	5698	11.8	5.35	0.589	0.063 and 0.109	2-Row Spheres	3.1 and 6.5	3
			4.25					30
			3.61					44
	5695	12.6	3.21	Sharp	Smooth	No	Trips	24
	5696	11.2	5.22	0.589	Smooth	No	Trips	45

Tunnel	Data Group	M_∞	Re_∞/ft x 10^{-6}	r_n, in.	k, in.	Type Trip	Extent, s/r_n Range	s_t, in.
B	1	8.0	3.4	0.589	0.014	Distributed Grit	0.20–15.0	3
	3		3.0					3
	9	8.0	3.7	0.589	0.014	Distributed Grit	0.20–10.4	3
	10		3.4					3
	11		3.0					8
	12		2.8					20
	14	8.0	3.4	0.589	0.014	Distributed Grit	0.80–5.0	3
	13		3.0					14
	33	8.0	3.7	0.295	0.010	Distributed Grit	0.80–5.0	4
	34		3.4					20
	35		3.0					Transition
	36		2.8					Laminar
	37	8.0	3.0	0.589	0.025	NCM	0.10–5.0	4
	38		2.5					10
	39		2.0					41
	4	8.0	3.8	0.589	0.014	NCM	0.10–5.0	3
	5		3.4					8
	6		3.0					22
	7		2.8					40
	44	8.0	3.7	2.187	0.025	Distributed Grit	0.20–5.0	2.2
	43		3.4					
	42		3.0					
	41		2.5					
	40		2.0					

Tunnel	Data Group	M_∞	Re_∞/ft x 10^{-6}	r_n, in.	k, in.	Type Trip	Extent, s/r_n Range	s_t, in.
B	45	8.0	3.7	2.187	0.025	Distributed Grit	0.44-5	2.2
	46						0.78-5	2.8
	47						1.13-5	4.2
	48				Smooth	No	Trips	Laminar
	17	8.0	3.7	0.589	0.025	1-Row Spheres	3.1	Laminar
	24				0.063		3.1	6
	23				0.063		6.5	11
	20				0.078		13	19
	21				0.093		20	21
	22				0.109		33	25
	18	8.0	3.7	0.589	0.025 and 0.063	2-Row Spheres	3.1 and 6.5	13
	19				0.25, 0.063, 0.078	3-Row Spheres	3.1, 6.5, 13.0	7
	25	8.0	3.7	0.589	0.025	1-Row Spheres	6.5	Laminar
	26				0.047			23
	27				0.109			4.0
	31	8.0	3.7	0.295	0.039	1-Row Spheres	6.5	Laminar
	32				0.063		13	15
	15	8.0	3.7	0.589	Smooth	No	Trips	Laminar
	30	8.0	3.7	0.295	Smooth	No	Trips	Laminar
	28	8.0	3.7	Sharp	Smooth	No	Trips	17

NOMENCLATURE

h_o	Total enthalpy
k	Trip element height, in.
M_e	Mach number at edge of boundary layer
M_∞	Free-stream Mach number
$N_{st,\infty}$	Stanton number based on free-stream conditions
P	Pressure, psia
P_o'	Free-stream pitot pressure, psia
P_o	Reservoir pressure, psia
p_∞	Free-stream pressure, psia
q_∞	Free-stream dynamic pressure, psia
$\dot{q}$	Heat-transfer rate, Btu/ft^2-sec
$\dot{q}_o$	Stagnation point q based on model radius, Btu/ft^2-sec
Re_∞/ft	Reynolds number based on free-stream conditions and a one-foot length
r_b	Model base radius, in.
r_n	Model nose radius, in.
s	Surface distance along the model measured from the stagnation point, in.
s_∞	Free-stream entropy
T_w	Model wall temperature, °R
T_∞	Free-stream temperature, °R
T_{o_∞}	Free-stream total temperature, °R
x	Axial distance along the model measured from the sharp apex, in.
R	Gas constant

δ_k Boundary-layer thickness at the trip

δ^* Boundary-layer dispacement thickness (not necessarily at the sonic point)

θ_c Cone half-angle, deg

ϕ Model circumferential angle, deg

SUBSCRIPTS

e Boundary-layer edge conditions

k At trip location

t At the end of transition

∞ Free-stream conditions